Climate Dynamics
https://doi.org/10.1007/s00382-023-06706-w

Can global warming bring more dust?

Yumeng Zhou[1,2] · Tongwen Wu[1,2,3] · Yang Zhou[4] · Jie Zhang[2,3] · Fang Zhang[2,3] · Xiaole Su[5,6] · Weihua Jie[2,3] · He Zhao[2,3] · Yanwu Zhang[2,3] · Jun Wang[7]

Received: 30 June 2022 / Accepted: 6 February 2023

Abstract

In the late twentieth century, global mean surface air temperature especially on land is continuously warming. Our analyses show that the global mean of dust increased since 1980, using the Modern-Era Retrospective Analysis version 2 for Research and Applications (MERRA-2) reanalysis data. This variation of global dust is mainly contributed by the dust increase outside of dust core areas (i.e. high dust mass concentration region). The causes to result in global dust variations are explored. In dust core areas, surface wind is the primary driving factor for surface dust, both of which show no remarkable trends of increase or decrease since 1980. In areas outside of the core areas, especially in arid and semi-arid areas in North and Middle Asia, surface air temperature warming is the primary impact factor causing the dust increase. An increase in surface air temperature is accompanied by enhancement of atmospheric instability which can trigger more upward motion and bring more dust. All 9 Earth System Models (ESMs) for the Aerosol Chemistry Model Intercomparison Project (AerChemMIP) reproduce the reasonable spatial distribution and seasonal cycle of dust in the present day. But only a few models such as BCC-ESM1 and GFDL-ESM4 simulate the increasing trend of dust similar to MERRA-2. While the primary impact of wind in dust core areas, and surface temperature outside of the core areas, especially in middle to high latitudes in Eurasian continent, are presented in most ESMs.

Keywords Dust aerosols · Global warming · CMIP6 · Earth system models

1 Introduction

Recently, severe dust events have occurred frequently worldwide. For example, there are seven dust events occurred in the Sistan and Lake Harmon basin areas in the last 20 years (Rami et al. 2022); an extraordinary dust storm engulfed the Khuzestan province in Iraq, damaged the electricity infrastructure and even triggered the disruption of electricity supply in cities such as Awash (Ledari et al. 2022); three strong dust events occurred in southern Iran in the winter and spring of 2018 (MalAmiri et al. 2022); a severe sandstorm occurred in the Sahara Desert of North Africa in June 2020, affecting an Atlantic hurricane that year (Francis et al. 2022); three extremely wide-ranging sandstorms occurred in Beijing in March 2021 (Filonchyk 2022; Wang et al. 2021); and a strong dust event occurred in Iraq on April 7–9, 2022 (https://earthobservatory.nasa.gov/images/149695/dust-storm-in-iraq). Dust increasing may be caused by various factors such as surface wind speed, precipitation, soil moisture, temperature, and water resources (Gillette and Passi 1988; Hamidi et al. 2017; Hamidi 2020; Shi et al.

✉ Tongwen Wu
twwu@cma.gov.cn

1 Chinese Academy of Meteorological Sciences, China Meteorological Administration, Beijing 100081, China

2 CMA Earth System Modeling and Prediction Center (CEMC), China Meteorological Administration, Beijing 100081, China

3 State Key Laboratory of Severe Weather, Chinese Academy of Meteorological Sciences, Beijing 100081, China

4 Key Laboratory of Meteorological Disaster, Ministry of Education, Collaborative Innovation Center on Forecast and Evaluation of Meteorological Disasters, Nanjing University of Information Science and Technology, Nanjing 210044, China

5 Henan Provincial Climate Centre, Zhengzhou 450003, China

6 Henan Key Laboratory of Agrometeorological Support and Applied Technique, China Meteorological Administration, Zhengzhou 450003, China

7 Department of Chemical and Biochemical Engineering, The University of Iowa, Iowa City, IA 52242, USA

Published online: 22 February 2023

2021; Sissakian et al. 2013). Does the frequent occurrence of severe dust events is related to the global warming?

Many studies have shown that the dust variations exist in their regional dependence in the twentieth century of global warming. The growth of the Earth's surface temperature can lead to surface evaporation increasing and the relative humidity decreasing, which dries the land, accelerates the surface soil disturbance, exacerbates the vegetation degradation, and then rises the possibility of dust emission (Goudie and Middleton 2001; Middleton and Kang 2017; Mirzabaev et al. 2019; Harrison et al. 2001; Munson et al. 2011; Wu et al. 2020b). There are evident increasing trends of dust concentration and dust storm frequency in North Africa, the eastern Mediterranean, Arabian Peninsula, and Middle East (Hamidi 2020; Middleton 1985; Goudie and Middleton 1992; Mbourou et al. 1997; Ganor et al. 2010; Notaro et al. 2015; Krasnov et al. 2016; Sissakian et al. 2013). In addition, the dust aerosol optical depth and dust emission flux in East Asia also showed an increasing trend from 1986 to 2005 (Zong et al. 2021). However, the frequency of dust activities has decreased significantly for the average of North and South Africa, Northeast Asia, Central Asia, and northern China, in recent years (Shao et al. 2013; Indoitu et al. 2012; Song et al. 2016; Zhu et al. 2008). This decrease in dust is explained by the decrease in local wind speed (Tsunematsu et al. 2011; Zhang et al. 2003; Zhu et al. 2008), and it is suggested that the temperature difference between the polar and equatorial regions decreases under the influence of global warming, so that the pressure gradient decreases, resulting in the reduction of wind speed, which may reduce dust emissions and the frequency of dust events.

With the development of numerical models in recent years, the Earth System Model (ESM) has been a complex model system used to describe the formation, emission, transportation, gas-phase chemical reaction, deposition, and other processes of various aerosols, including dust aerosols and atmospheric chemical components (Dunne et al. 2020; van Noije et al. 2021; Wu et al. 2020a). The ESM is an important tool to study the outbreak of global and regional dust events and variations in dust concentrations with global warming. The Aerosol Chemistry Model Intercomparison Project (AerChemMIP, Collins et al. 2017), endorsed by the Coupled Model Intercomparison Project (CMIP6, Eyring et al. 2016), designs the historical experiment, where the external forcing fields used in ESMs include CO_2, CH_4, N_2O, and other greenhouse gas concentrations, solar radiation, volcanic activity, while other chemical species including dust aerosols and from anthropogenic emissions. This experiment provides important simulation data for our study to explore the global atmospheric dust concentration changes in recent decades.

Therefore, the purpose of this study is to explore the regional feature of dust variation since 1950 and the relationships between dust and temperature, wind, and soil moisture. The data used in this study are introduced in Sect. 2, the main results are shown in Sect. 3, and the summary and discussion are presented in Sect. 4.

2 Data

The monthly MERRA-2 reanalysis data with a resolution of 0.5° lat × 0.625° lon from 1980 to 2020, including dust concentration in the whole column and that near the surface (GMAO 2015, https://disc.gsfc.nasa.gov/datasets?project=MERRA-2, last access: 20 January 2022), are used to explore the global variations of dust. Those are the longest global dust series that we can access currently. The MERRA-2 data integrates observations from multiple sources, such as the Moderate Resolution Imaging Spectroradiometer (MODIS), the Advanced Very High Resolution Radiometer (AVHRR), the Multi-angle Imaging Spectro Radiometer (MISR), and the Aerosol Robotic Network (AERONET) (Gelaro et al. 2017; Randles et al. 2017; Rienecker et al. 2011). The MERRA-2 reanalysis data provided an important basis that is widely used by researchers on dust in Africa (Grogan and Thorncroft 2019; Prospero et al. 2020; Veselovskii et al. 2018), West Asia (Hamidi 2020; Roshan et al. 2019; Ukhov et al. 2020; Yousefi et al. 2020), East Asia (Qin et al. 2018; Yao et al. 2020, 2021), and Australia (Mukkavilli et al. 2019).

Three sets of 1980–2020 monthly gridded reanalysis data are used to analyze the relationships between dust and temperature, wind, and soil moisture. They include: (1) the global monthly air surface temperature with the resolution of 0.5° lat × 0.5° lon from Climatic Research Unit gridded Time Series version 4.05 (CRU TS4.05, https://catalogue.ceda.ac.uk/uuid/c26a65020a5e4b80b20018f148556681, last access: 19 March 2022), which is based on terrestrial observations (Harris et al. 2020, 2021), and widely used to study the variation of surface temperature (e.g., Karim et al. 2020; Xu et al. 2020); (2) global 0.5° lat × 0.5° lon monthly data of temperature and wind speed at pressure levels from the European Centre for Medium-Range Weather Forecasts (ECMWF) Reanalysis v5 (ERA5, https://www.ecmwf.int/en/forecasts/datasets/reanalysis-datasets/era5, last access:

21 March 2022), which is a comprehensive reanalysis data using the 4D-Var data assimilation and model forecasts in CY41R2 of the ECMWF Integrated Forecast System (Hersbach et al. 2019a, 2019b, 2020), and widely used in many researches (e.g., Jiang et al. 2021; Zhu et al. 2021); and (3) the global monthly upper soil (0–10 cm) water contents with the resolution of 2.5° lat × 2.5° lon from the Global Land Data Assimilation System (GLDAS, https://disc.gsfc.nasa.gov/datasets/GLDAS_NOAH025_M_2.1/summary?keywords=GLDAS, last access: 21 March 2022), which is developed by NASA's Goddard Space Flight Center (GSFC) in conjunction with the National Oceanic and Atmospheric Administration (NOAA) and the National Centers for Environmental Prediction (NCEP) and using new generation of ground and satellite observation systems and advanced land surface modeling and data assimilation techniques to ingest satellite- and ground-based observational data products (Beaudoing et al. 2020; Rodell et al. 2004), providing an important and reliable data to study soil moisture (e.g., Fu and Wang 2014; Kędzior and Zawadzki 2016). In order to validate the impact of the surface temperature, wind speed, and soil moisture on dust variation, we also use those data from the same source of MERRA-2.

The 1950–2014 monthly gridded data from historical simulations of 9 ESMs (listed in Table 1) for AerChemMIP, including the dust aerosol mass mixing ratio, air temperature, surface wind speed, and upper soil (0–10 cm) water content, are used in this study to evaluate the performance of the ESMs and also verify our diagnostic analyses derived from observations.

To facilitate the comparative analysis of each data, all the data are interpolated to grid points with a horizontal resolution of 1° lat × 1° lon in this study.

3 Results

3.1 Present-day climate of dust aerosol simulations in ESMs

Figure 1 shows the spatial distribution of the annual mean dust aerosol column concentrations of MERRA-2 and the 9 ESMs and their multi-model mean (MME) from 1995 to 2014. Dust aerosols have remarkable regional characteristics in MERRA-2 (Fig. 1a), mainly concentrating in the "dust belt" that extends from North Africa to East Asia via the Middle East, Central Asia, and South Asia (0°–130° E, 0°–60° N). High concentration areas are mainly located in arid regions, such as the Sahara Desert in Central and North Africa, the Arabian Peninsula in the Middle East, and the Taklimakan Desert in East Asia. The conclusions above are consistent with previous research (Ginoux et al. 2001, 2012; Zender 2003). All the ESMs can basically reproduce the spatial distribution characteristics of dust aerosols with high spatial correlation coefficients over 0.67, and the spatial correlation coefficient between the MME and MERRA-2 is even up to 0.95.

The seasonal cycle of the global (60° S to 90° N) mean dust concentrations averaged for the period during 1995–2014 is presented in Fig. 2. The dust burden in the atmosphere from MERRA-2 shows an obvious seasonal variation, higher in boreal spring and summer from March to June and lower in winter from November to January. Most models and the MME can basically capture those seasonal variation characteristics, except for MIROC-ES2L (in which the high value is in July).

3.2 Variation in dust since 1950

To analyze the evolution of dust in recent years, Fig. 3 presents the globally-averaged annual mean of column mass density (DstDen, black line) and surface mass concentration (SurDst, red line) of dust over land since 1950. Their year-to-year variations resemble each other. From 1980 to 2020, MERRA-2 shows a significant increasing trend of dust (Fig. 3a). Especially from 1980 to 2010, the DstDen increased by 15 mg m^{-2} and the SurDst increased by 6 μg m^{-3}. For the 9 ESMs, only a few can show an analogous increasing trend, such as BCC-ESM1 (Fig. 3b) and GFDL-ESM4 (Fig. 3e), although increases in these models are much weaker than in MERRA-2. In most models, the trends of dust in the same period are negative, and are opposite to the MERRA-2, showing an evident decrease. Especially in EC-Earth3-AerChem and CESM2-WACCM, the DstDen decreases by 8–10 mg m^{-2}, and the SurDst decreases by 4–5 μg m^{-3}. As for the UKESM1-0-LL, the DstDen of UKESM1-0-LL increases by 3 mg m^{-2} while the SurDst decreases by 3 μg m^{-3} during 1980–2010. The DstDen and SurDst of UKESM1-0-LL are consistent before 2000, but opposite variations after 2000.

Figure 4 shows the geographical distribution of the linear trend of 1980–2010 annual means of SurDst on global land. The MERRA-2 data shows a significant growth trend over most of the global land, especially in northeastern North Africa, the Arabian Peninsula, east of the Taklimakan Desert in East Asia, and near the Himalayas in northern South Asia.

Table 1 CMIP6 Earth system models used in this study

Model	Institution	Model resolution	Vert levels (top level)	Aerosol components	Dust size diameter boundaries (µm)	Dust emission scheme	Model and data references
BCC-ESM1	BCC (Beijing Climate Centre), China	2.813° × 2.813°	L26 (42 km)	BCC-AGCM3-Chem (Wu et al. 2020a)	4 bins: 0.1–1.0, 1.0–2.5, 2.5–5.0, 5.0–10.0	Zender (2003)	Wu et al. (2020a) and Zhang et al. (2018)
CESM2-WACCM	NCAR (National Center for Atmospheric Research), U.S.A	0.938° × 1.25°	L70 (80 km)	MAM4 (Liu et al. 2016)	3 modes: 0.01–0.1, 0.1–1.0, 1.0–10.0	Zender (2003)	Danabasoglu (2019) and Danabasoglu et al. (2020)
EC-Earth3-AerChem	EC-Earth-consortium, Europe	0.703° × 0.703°	L34 (36 km)	TM5 (van Noije et al. 2014, 2021)	3bins: 0.03–0.55, 0.55–9.0, 9.0–20	Marticorena and Bergametti (1995)	EC-Earth Consortium (EC-Earth) (2020) and van Noije et al. (2021)
GFDL-ESM4	NOAA-GFDL (National Oceanic and Atmospheric Administration, Geophysical Fluid Dynamics Laboratory), USA	1.25° × 1°	L49 (80 km)	GFDL-AM4.1 (Horowitz et al. 2020)	5 bins: 0.1–1.0, 1.0–2.0, 2.0–3.0, 3.0–6.0, 6.0–10.0	Evans et al. (2016)	Dunne et al. (2020) and Krasting et al. (2018)
GISS-E2-1-G	NASA-GISS (Goddard Institute for Space Studies), U.S.A	2° × 2.5°	L40 (66 km)	OMA (Bauer et al. 2020)	6 bins: < 1.0, 1.0–2.0, 2.0–4.0, 4.0–8.0, 8.0–16.0,16.0–32.0	Cakmur et al. (2006); Miller et al. (2006)	Kelley et al. (2020), NASA Goddard Institute for Space Studies (NASA/GISS) (2018)
MIROC-ES2L	MIROC consortium (JAMSTEC, AORI, NIES, R-CCS), Japan	2.813° × 2.813°	L40 (40 km)	SPRINTARS6.0 (Takemura 2005; Takemura et al. 2000, 2009)	6 bins: 0.1–0.16, 0.16–0.25,0.25–0.40, 0.40–0.63, 0.63–1.0, 1.0–1.58, 1.58, 2.51,2.51–3.98, 3.98–6.31, 6.31–10.0	Takemura et al. (2000)	Hajima et al. (2019, 2020)
MPI-ESM-1-2-HAM	HAMMOZ-Consortium, Switzerland, Germany, UK, Finland	1.875° × 1.875°	L47(80 km)	HAM2.3 (Tegen et al. 2019)	3 bins in sub-range 1 (0.003–0.05), 2×4 bins in sub-range 2 (0.05–0.73), 3×3 bins in sub-range 3 (0.73–10.0)	Tegen et al. (2002)	Neubauer et al. (2019) and Tegen et al. (2019)
NorESM2-LM	NCC (NorESM Climate Modelling Consortium), Norway	1.875° × 2.5°	L32(40 km)	OsloAero (Kirkevåg et al. 2018; Seland et al. 2020)	3 modes: 0.01–0.1; 0.1–1.0; 1.0–10.0	Zender (2003	Seland et al. (2019, 2020)
UKESM1-0-LL	MOHC (Met Office Hadley Centre), UK	1.25° × 1 °	L85(85 km)	UK-GLOMAP (Mulcahy et al. 2020)	6 bins: 0.064–0.2, 0.2–0.63, 0.63–2.0, 2.0–6.32, 6.32–20.0, 20.0–63.0	Marticorena and Bergametti (1995), and Woodward (2001)	Sellar et al. (2019) and Tang et al. (2019)

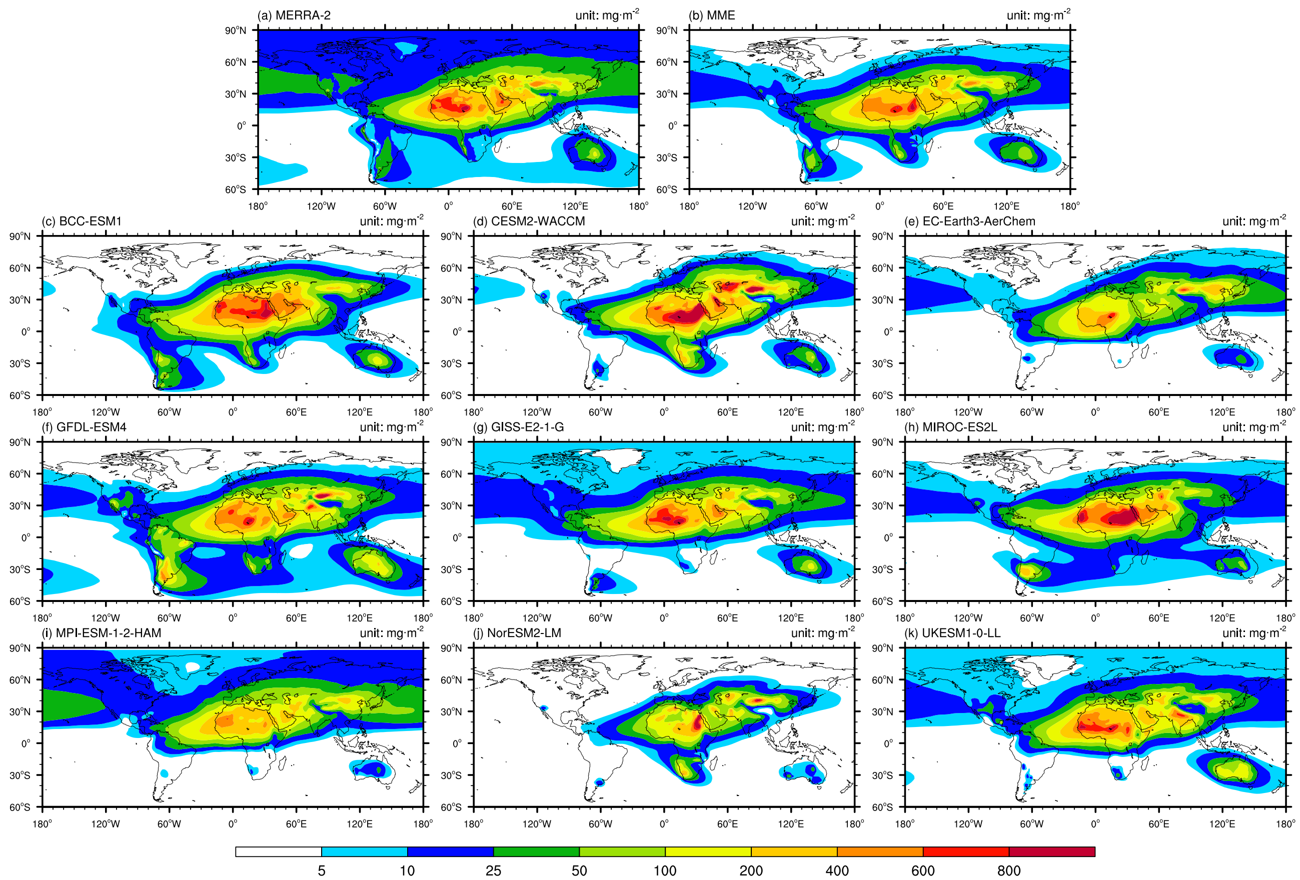

Fig. 1 Spatial distribution of annual mean dust aerosol column mass density for MERRA-2 (**a**) and the 9 ESMs (**c**–**k**) and MME (**b**) from 1995 to 2014. Unit: mg m^{-2}

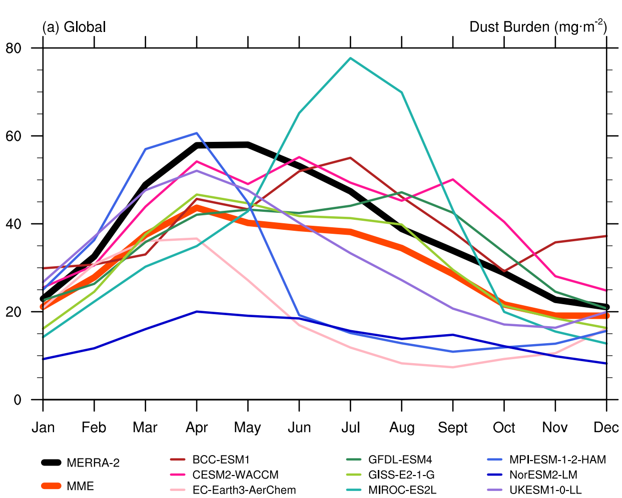

Fig. 2 The seasonal cycle of global mean dust burden averaged from 60° S to 90° N for MERRA-2 (black line), 9 ESMs (colorful lines), and their MME (red line) during the period of 1995–2014. Unit: mg m^{-2}. Considering the low dust burden south of 60° S, global mean results in this study refer to the average from 60° S to 90° N

Moreover, the SurDst in regions such as North and South America and the coast of Australia also increases significantly. The increasing SurDst from MERRA-2 in some regions (Fig. 4a) is also caught from other observations data. For example, utilizing MODIS images data, Bin Abdulwahed et al. (2019) found that the frequency, spatial extent, and intensity of dust storms in the Middle East increases in the last 15 years from 1997 to 2012.

As in Fig. 4a, MERRA-2 data also shows a decrease in several regions such as in the Sahel of North Africa, North China, and central Australia, where the dust exists in the period from 1980 to 2010. There are previous studies to prove dust decrease in those regions utilized other data. For example, using aerosol optical depth (AOD) at 380 nm from the Total Ozone Mapping Spectrometer (TOMS), Foltz and McPhaden (2008) showed that the dust in the Sahel region decreases obviously from 1980 to 2006. Duan et al. (2022) used the “dust (storm) data set (v1.0)” established by the

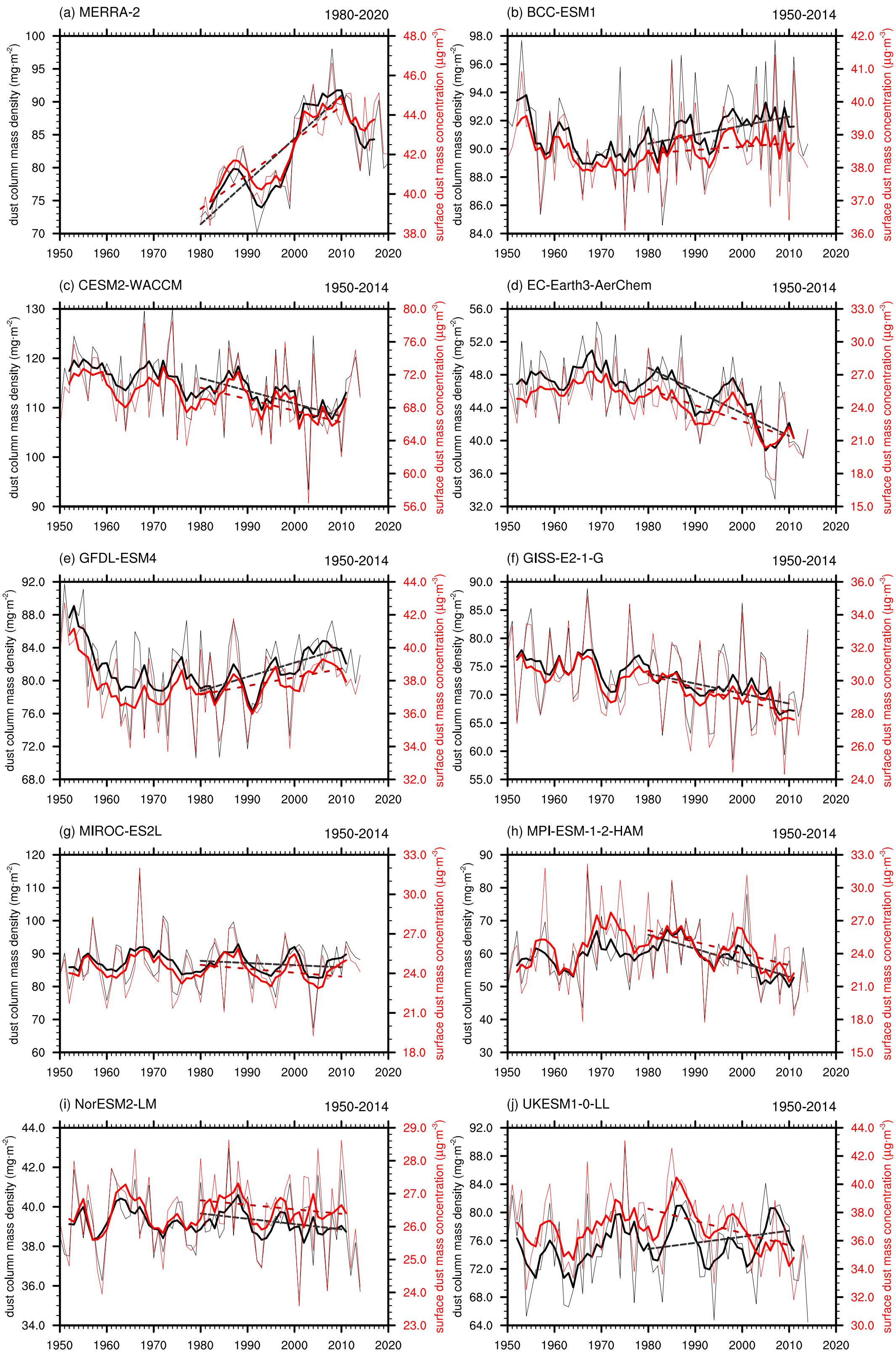

Fig. 3 The global (60° S–90° N) average of annual mean of dust aerosols column mass density (black line, unit: mg m^{-2}) and surface dust aerosols mass concentration (red line, unit: μg m^{-3}) for MERRA-2 (**a**) and 9 ESMs (**b–j**). Thick lines show the 5-year smooth for the annual data (thin lines)

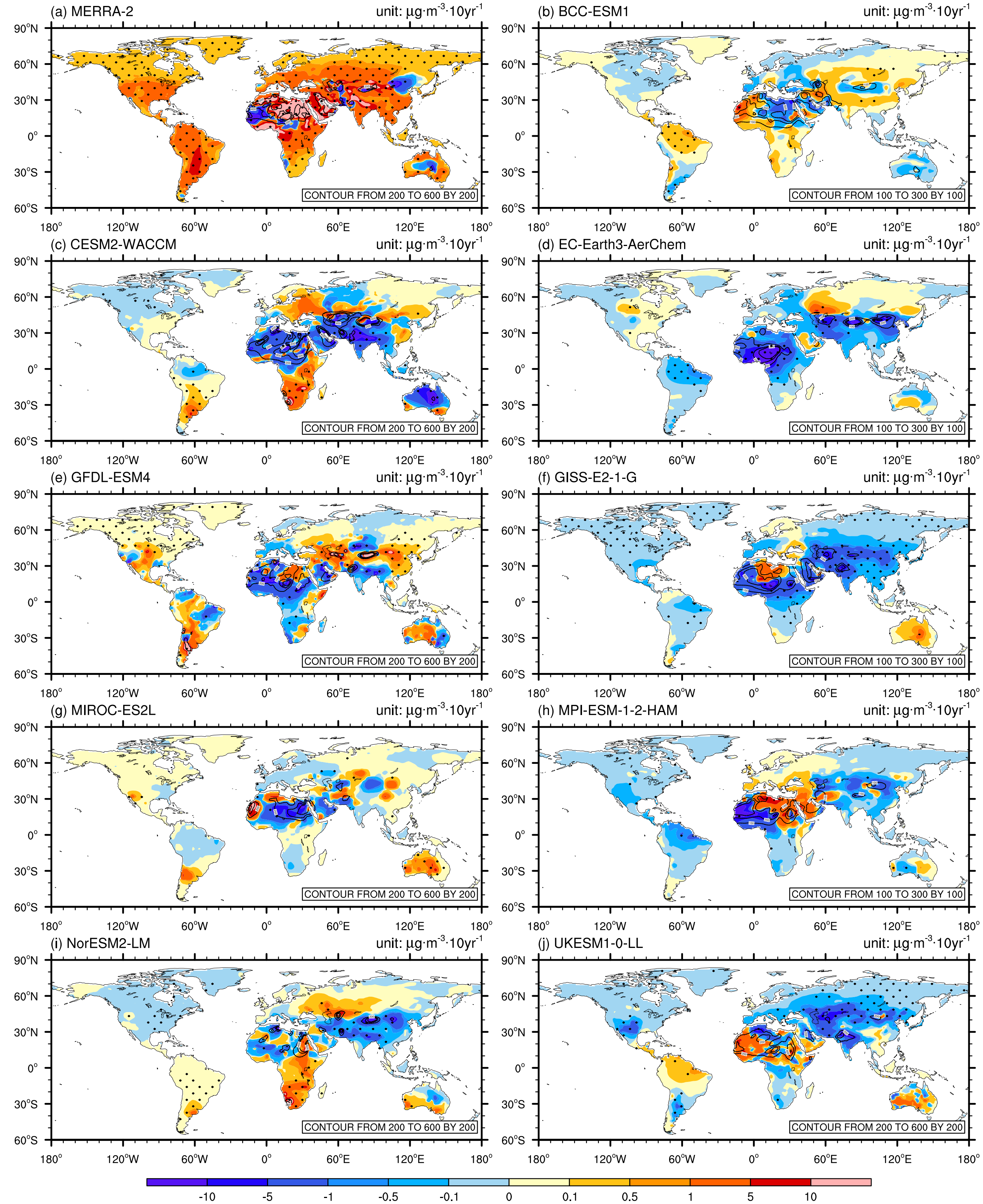

Fig. 4 The spatial distribution of linear trend coefficient of surface dust aerosol mass concentration (μg m^{-3} 10 year^{-1}) on global land from **a** MERRA-2, and **b**–**j** 9 ESMs during the period of 1980–2010. Values significant at the 95% level using a student's t test are stippled. Contours show the 1980–2010 averaged mean of monthly surface dust aerosol mass concentration (μg m^{-3})

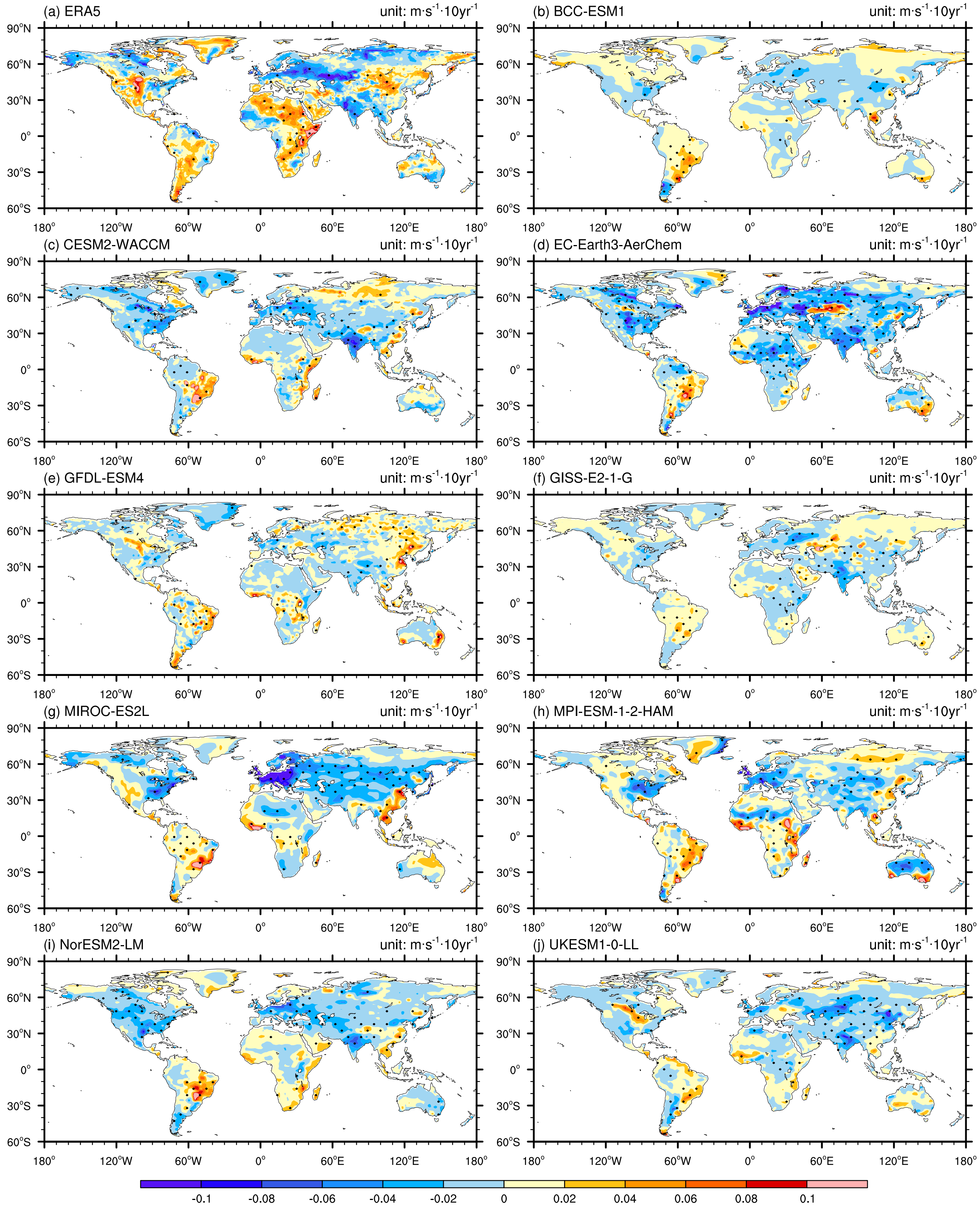

Fig. 5 The spatial distribution of linear trend coefficient of surface wind speed (m s^{-1} 10 year^{-1}) on global land from **a** MERRA-2, and **b**–**j** 9 ESMs during the period of 1980–2010. Values significant at the 95% level using a student's t test are stippled

meteorological information center of the China Meteorological Administration to suggest the annual number of sand-dust processes in China decreased significantly from 1960 to 2020.

The spatial distributions of the linear trend coefficients of the SurDst in the 9 ESMs are very different. To some extent, BCC-ESM1, GFDL-ESM4, and NorESM2-LM can partly capture the increasing trend of surface dust in the middle and high latitude regions around the Taklimakan Desert in Asia and a decreasing trend in the core areas of high SurDst in North Africa.

Some previous studies (Tsunematsu et al. 2011; Zhang et al. 2003; Zhu et al. 2008) suggested the global warming decreases surface wind speed and dust concentration. Here, we further explore the distribution of the linear trend of 1980–2010 annual means of the surface wind speed from ECWMF on global land (Fig. 5). It shows that surface wind speed obviously decreased in most part of Europe, and South Asia, but increased in most parts of Africa and East Asia. It is interesting that 9 ESMs simulated surface wind decrease in most regions of global land in the period of 1980–2010 (Fig. 5b–j). Therefore, the change of surface wind speed cannot reasonably account for the SurDst variation in every region as shown in Fig. 4.

3.3 Possible reasons for SurDst changes

As shown in Fig. 6a, the average global mean CRU surface air temperature over land increases significantly since 1980 (red line, Fig. 6a), increasing by approximately 1 °C

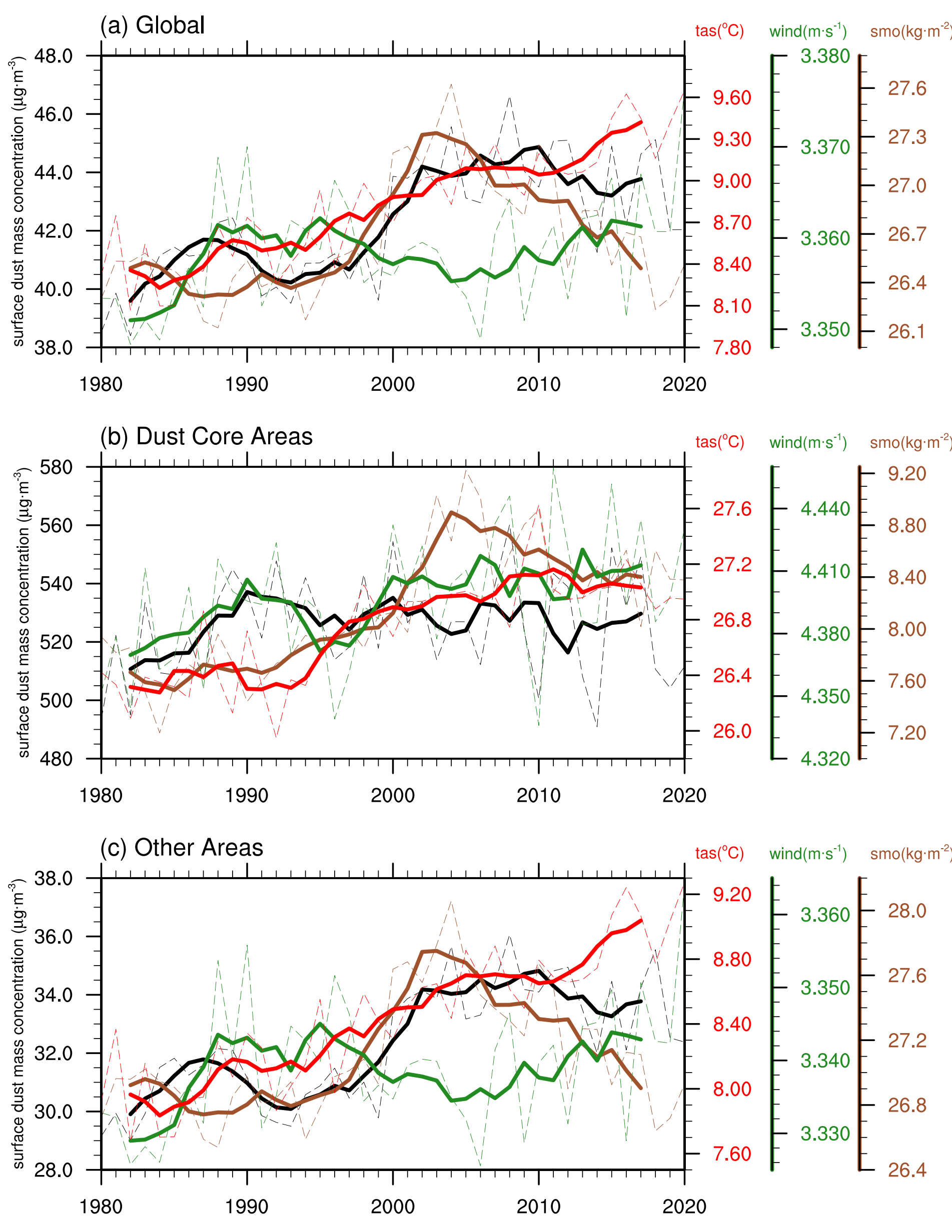

Fig. 6 Variation of land surface dust aerosols mass concentration (black lines, μg m^{-3}), surface air temperature (red lines, units: °C), surface wind speed (blue lines, m s^{-1}), and soil moisture (brown lines, kg m^{-2}) averaged for **a** global (60° S–90° N), **b** dust core areas (the 1980–2020 averaged mean of monthly surface dust aerosols mass concentration more than 400 μg m^{-3}) and **c** other areas during the period of 1980–2020. Solid lines show the 5-year smooth for the annual data (dotted lines) from 1980 to 2020

over 41 years, which is consistent with the Sixth Assessment Report of the International Panel on Climate Change (IPCC 2022). The increasing trend of SurDst in MERRA-2 (black line, Fig. 6a) is highly consistent with the warming in surface air temperature, and the correlation coefficient of their 5-year smoothing series reaches 0.84, which passes the 99% significance test. However, the relationship between the SurDst and global land averaged surface wind speed of ERA5 (green line, Fig. 6a) is insignificant, and the variation of wind speed even shows an opposite trend in contrast to the SurDst in 1995–2005. It is also unexpected that the soil moisture of GLDAS (brown line, Fig. 6a) shows a consistent growth trend with the SurDst, especially during 1990–2000 with the correlation coefficient of the 5-year smoothing series of 0.83. It seems that the globally-averaged wind near surface and soil moisture do not reasonably account for the global mean dust variation.

If we classified the dust core areas as the regions with the annual mean SurDst greater than 400 μg m^{-3} over land, their different variations in surface dust concentrations, wind, and soil moistures between in dust core areas and other regions are clear. This definition of the dust core areas is consistent with previous studies based on ground-based dust observations and remote sensing data using retrospective and frequency methods (Ginoux et al. 2010; Middleton and Goudie 2001; Prospero et al. 2002; Schepanski et al. 2012). As shown in Fig. 6b, the interannual variability of the SurDst in the core areas (black line, Fig. 6b) is relatively large, but it does not show a significant increasing trend and basically remains at approximately 520 μg m^{-3}. The interannual variation and trend of the SurDst are closely related to the surface wind speed (green line, Fig. 6b), whose correlation coefficient reaches up to 0.79 after detrending, and up to 0.56 for 5-year smoothing series, both of which pass the 99% significance test. Especially in the period from 1980 to 1990, the increase in surface wind speed is highly consistent with the enhancement of the SurDst in the core areas (Fig. 6b). We noted that surface wind speed still keeps a slight increase since 1990 in the core areas, but there is no obvious variation of dust over there, which is partly caused by the negative effect of enhancement in soil moisture to inhibit the dust increase. The interannual variations of wind and dust still keep a high correlation (0.78) in this period. In other regions out of dust core areas (Fig. 6c), the variations of dust, wind, and soil moisture since 1980 are basically consistent with the global means (Fig. 6a), and there is a high positive correlation between dust mass and the surface air temperature.

Figures 7, 8, and 9 show the spatial distributions of the relationship between SurDst and the three key variables including surface wind speed, soil moisture, and surface air temperature on the “dust belt” (0°–130° E, 0°–60° N) where the monthly SurDst higher than 10 μg m^{-3}. As shown in Fig. 7, the most significant positive correlation between the SurDst of MERRA-2 and the surface wind speed of ERA5 is in the dust core areas, such as North Africa, West Asia, and East Asia. This further verifies the conclusion that the SurDst in the core areas is highly correlated with wind speed (Fig. 6b). This conclusion can also be reflected in all the ESMs. For example, in BCC-ESM1, the significant positive correlation between the SurDst and surface wind speed is mainly located in the areas where the annual average SurDst is higher than 100 μg m^{-3} from 1950 to 2014, and it reaches as high as 0.8 where SurDst is higher than 300 μg m^{-3} in North Africa. The surface wind speed is a variable directly related to the dust emission process in the classical dust emission mechanism (Gillette and Passi 1988). Since the core areas are mostly desert areas with dry underlying surfaces, when the wind speed exceeds the critical friction velocity, the dust will be blown and enter the atmosphere to form the dust aerosol. Therefore, in the core areas, the higher the wind speed is, the higher the dust emission and the SurDst will be, which explains why the positive correlation between SurDst and surface wind speed is more significant there.

The SurDst and soil moisture are negatively correlated in most areas of the "dust belt" (Fig. 8). The most significant negative correlation in reanalysis data (Fig. 8a) is in southern North Africa and South Asia, with the lowest correlation coefficient reaching − 0.6. Almost all ESMs can verify the significant negative correlation in southern North Africa, while in other areas it is evidently different among ESMs. For example, in BCC-ESM1, the most significant correlation is in the south of high dust concentration area in East Asia, while in CESM2-WACCM, NorESM2-LM, GISS-E2-1-G, and UKESM1-0-LL, it is near South Asia. The negative correlation between the SurDst and soil moisture in MIROC-ES2L is significant in the entire "dust belt" (Fig. 8g), with the lowest correlation coefficient exceeding − 0.8. The difference in the relationship between surface dust and soil moisture in the ESMs may be one of the reasons for the difference in the dust evolution trends. It is worth noting that previous studies have shown that soil water content can reduce the wind erodibility of land (Chepil 1956; McKenna-Neuman and Nickling 1989), which can explain the negative correlation between soil moisture and SurDst.

Figure 9 shows the correlation between surface air temperature and dust. The significant positive correlation in

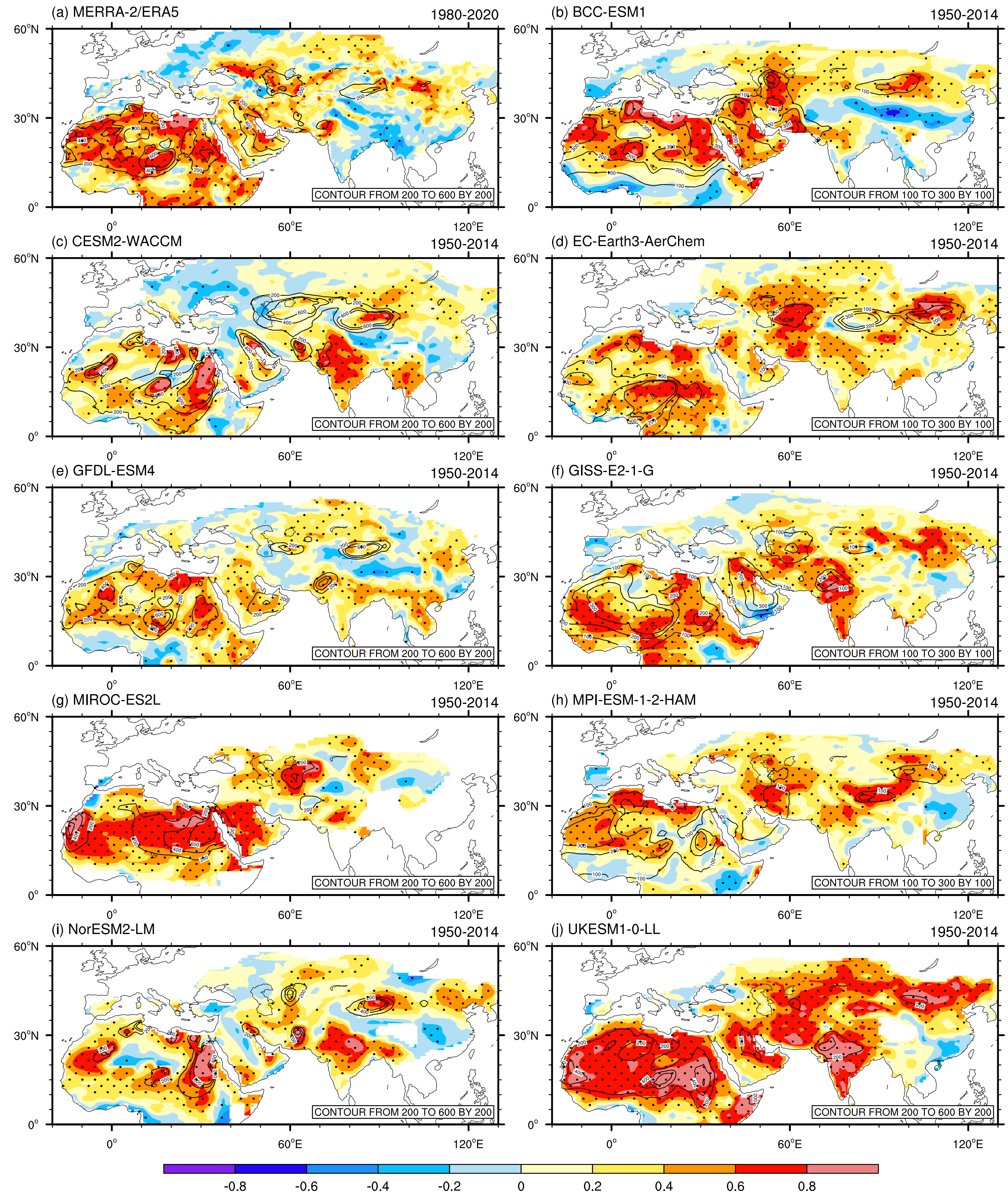

Fig. 7 Distribution of correlation coefficients between annual surface dust aerosols mass concentration (unit: μg m^{-3}) and surface wind speed (unit: m s^{-1}) for **a** MERRA-2/ERA5 during the period of 1980–2020 and **b**–**j** 9 ESMs during the period of 1950–2014. Values where all monthly surface dust aerosol concentrations are below 10 μg m^{-3} are masked, and values significant at the 95% level using a Student's t test are stippled. Contours show the 1980–2020/1950–2014 averaged mean of monthly surface dust aerosol mass concentration (unit: μg m^{-3})

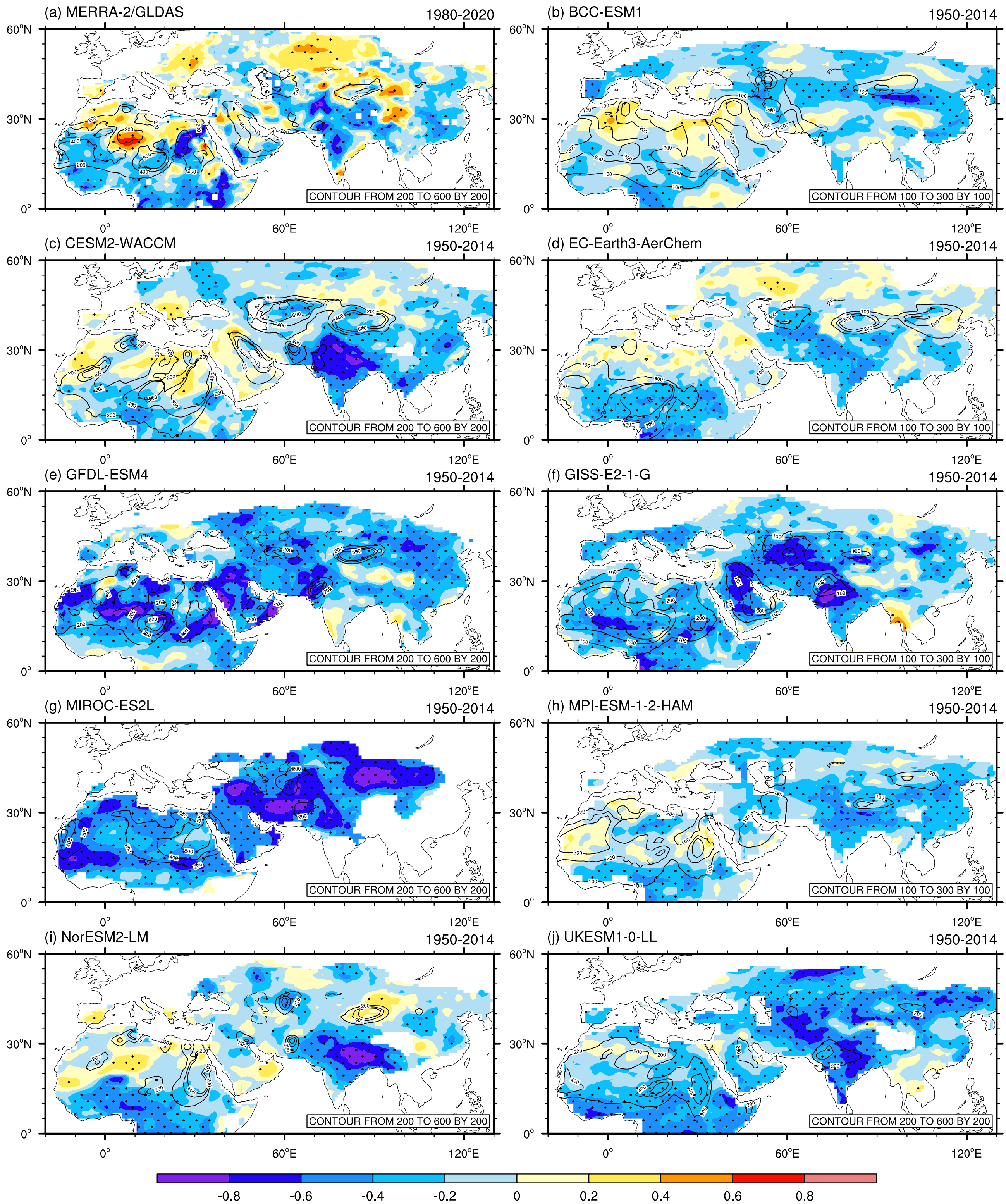

Fig. 8 Same as Fig. 7, but for correlation coefficients between annual surface dust aerosols mass concentration (unit: µg m^{-3}) and soil moisture (unit: kg m^{-2}). Observation data are from MERRA-2 and GLDAS

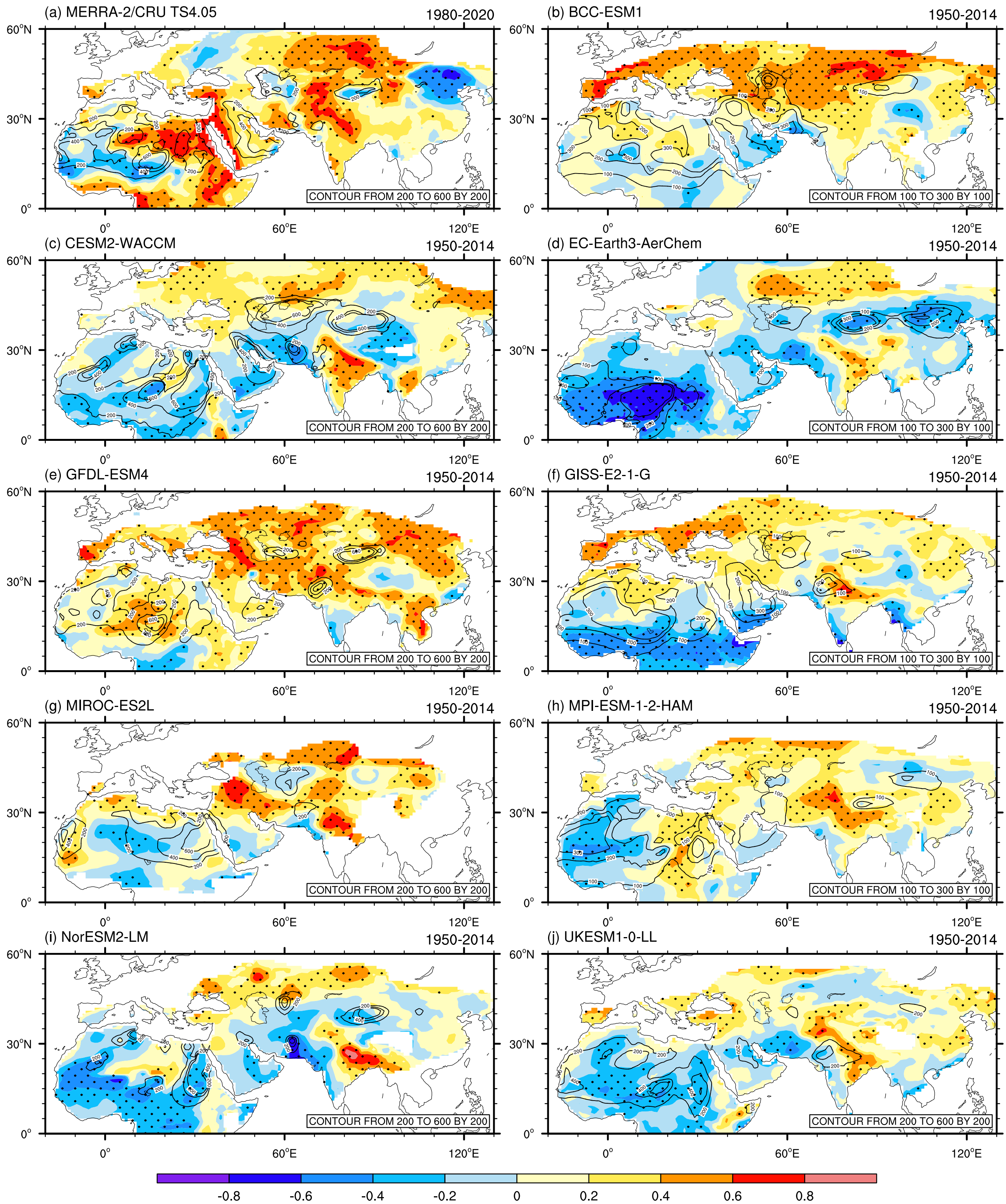

Fig. 9 Same as Fig. 7, but for correlation coefficients between annual surface dust aerosols mass concentration (unit: μg m^{-3}) and surface air temperature (unit: °C). Observation data are from MERRA-2 and CRU TS4.05

observation (Fig. 9a) is mainly manifested in the periphery of the dust core areas, such as northeast of the Sahel region in North Africa and the middle and high latitude regions of the Eurasian continent, where the correlation coefficient can reach 0.6, passing the 95% significance test. However, the correlation coefficients are negative over high SurDst regions in northern and northeastern China, and the Sahel region of North Africa. Most models also show that it is a significant positive correlation between the SurDst and surface air temperature in these arid and semiarid areas outside the core areas, especially in BCC-ESM1, GFDL-ESM4, GISS-E2-1-G, and MIROC-ES2L.

How to understand the in-phase variations for the SurDst and surface air temperature, and soil moisture (Fig. 6) and their positive correlation in the "dust belt" (Fig. 9)? We hypothesize the following connection chain. Warmer surface air temperature results in the increase of atmospheric instability in the lower troposphere. Increase in atmospheric instability will bring more dust emission especially in the arid and semiarid areas outside the core areas, and increase the lifetime of dust aerosols (and reduce the effect of dry deposition and gravitational settling) in semi-arid areas where the precipitation is always lacking. The studies of Hess and Spillane (1990) and Hess et al. (1988) shown that convection is a necessary condition for the dust emission process and initial formation of strong dust events. Increase in atmospheric instability will trigger more upward motion and bring more dust. However, a stronger upward motion may bring more precipitation and increase the soil moisture, especially in tropical regions, and then reduce the dust burden in the atmosphere. These two opposing effects depend on the relative importance of different factors on the dust in different regions and will be explored in the next section.

In order to test our hypothesis above, the difference between the surface air temperature and the air temperature at the top of layer with 150 hPa thickness above the ground is calculated, and is used as the vertical temperature gradient in the lower troposphere to represent the instability in the lower troposphere. Figure 10 presents the correlation distribution between the MERRA-2 SurDst and ERA5 vertical temperature gradient in a part of Asia (65° E–130° E, 20° N–60° N). It is clear that the correlation between the SurDst and the vertical temperature gradient in Asia is consistent with that between the SurDst and surface air temperature. The regions with significant positive correlation are mainly in arid and semiarid areas outside of dust core areas. Those relations are captured by a few models such as two ESMs (BCC-ESM1 and GFDL-ESM4).

3.4 Relative importance of wind, soil moisture, and air temperature to impact on dust

The multiple linear regression method suggested by Zhao et al. (2022) is used to objectively quantify the relative importance of three factors (including surface wind, soil moisture, and surface air temperature) on the SurDst in the "dust belt" (Fig. 11). The different colors in Fig. 11 represent different factors that dominate the SurDst at the grid point (surface air temperature (red), surface wind speed (green) and soil moisture (blue)), the darker color represents higher dominance. Here, only grid points with monthly average SurDst higher than 10 μg m^{-3} and whose regression coefficients pass the 95% significance test are shown. In MERRA-2, surface wind speed is the dominant driver of the SurDst in the dust core areas (such as western North Africa), while in the other areas, especially in the middle and high latitudes of the Eurasian Continent, the surface air temperature has a greater impact on the SurDst. Soil moisture is relatively important to the SurDst in only small-areas of regions, such as central South Asia and southern China, which also verifies the previous conclusion that soil moisture may have had little effect on the evolution of the SurDst in recent years. All the results are derived from different data sources. The relative importance of the surface temperature, wind speed, and soil moisture on the SurDst are verified by MERRA-2, and shown in Fig. 12. The consensus conclusions are conducted.

Almost all 9 ESMs can basically show that the surface wind speed is the dominant determinant of the SurDst in dust core areas. It is worth noting that surface air temperature is more important to the SurDst in the dust core areas in EC-Earth-AerChem, and UKESM1-0-LL shows that surface dust is mainly affected by wind in the entire dust belt, which is different from MERRA-2 and other models. Some models, such as BCC-ESM1, CESM2-WACCM, GFDL-ESM4, and GISS-E2-1-G, can verify the important role of surface air temperature on the SurDst in the middle and high latitudes of Eurasia. Except for MIROC-ES2L, most of the models show that soil moisture is the dominant factor to influence the SurDst just in some small areas, but these areas greatly differ among the models. Precipitation is closely related to soil moisture, and the relative importance of precipitation to effect on dust variation is consistent to that of the soil moisture (Figure omitted).

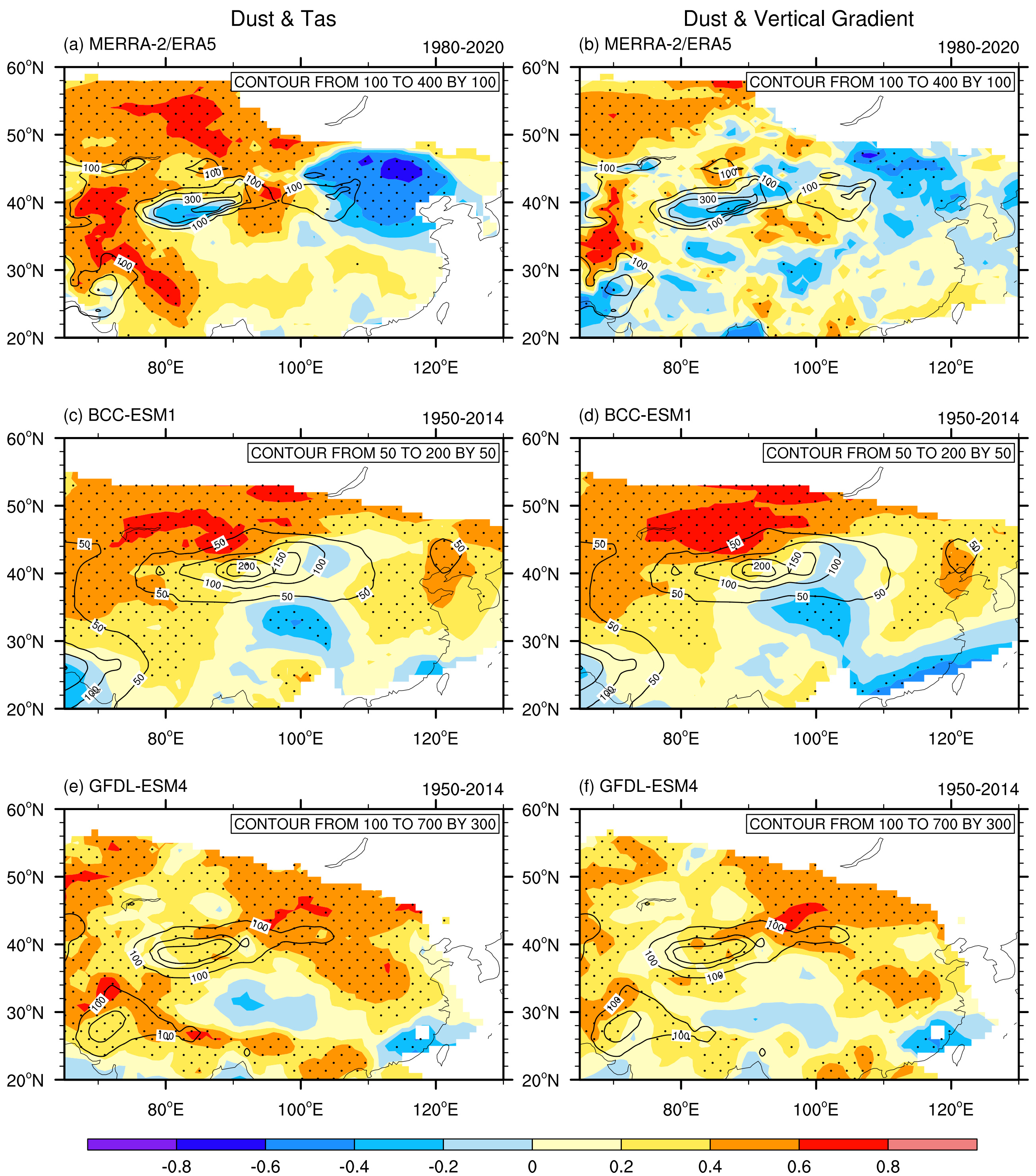

Fig. 10 Distribution of correlation coefficient between annual surface dust aerosols mass concentration and surface air temperature and temperature vertical gradient on lower atmosphere (the difference between the surface air temperature and the air temperature at the top of layer with 150 hPa thickness above the ground) in the east of Asia for **a**, **b** MERRA-2/ERA5 during the period of 1980–2020, **c**, **d** BCC-ESM1 and **e**, **f** GFDL-ESM4 during 1950–2014. Values where all monthly surface dust aerosol concentrations are below 10 μg m^{-3} are masked, and values significant at the 95% level using a student's t test are stippled. Contours show the 1980–2020/1950–2014 averaged mean of monthly surface dust aerosol mass concentration (unit: μg m^{-3})

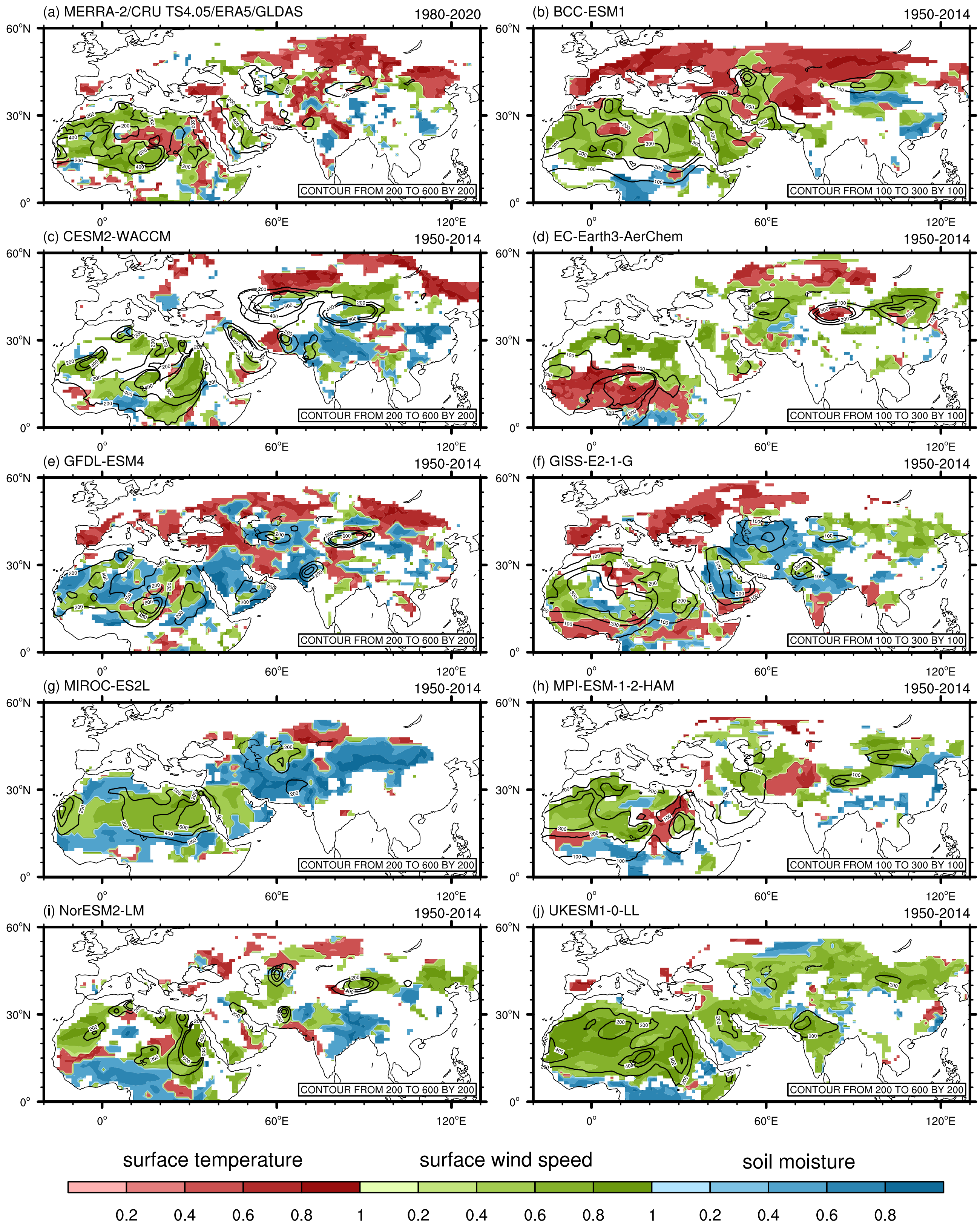

Fig. 11 Relative importance for the dominant factor of surface dust aerosol concentration (scaled to 0–1). Red masks for surface temperature, green for surface wind speed, and blue for soil moisture. Data used for regressions are 41 years (1980–2020) for MERRA-2/CRU TS 4.05/ERA5/GLDAS (**a**) and 65 years (1950–2014) for 9 ESMs (**b**–**j**). Values where all monthly surface dust aerosol concentrations are below 10 μg m^{-3} or not significant at the 95% level using a student's t test are masked

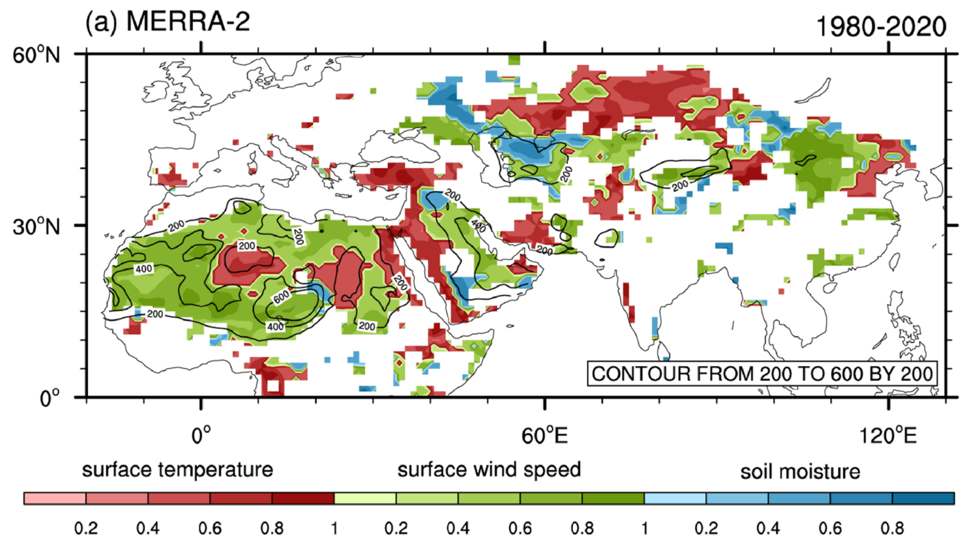

Fig. 12 Relative importance for the dominant factor of surface dust aerosol concentration (scaled to 0–1). Red masks for surface temperature, green for surface wind speed, and blue for soil moisture. Data used for regressions are 41 years (1980–2020) for MERRA-2. Values where all monthly surface dust aerosol concentrations are below 10 μg m^{-3} or not significant at the 95% level using a student's t test are masked

Overall, the surface wind speed is the dominant determinant of the SurDst in the dust core areas. In arid and semiarid regions around the core areas, especially in the middle and high latitudes of the Eurasian continent, the surface air temperature is the most important factor determining the SurDst. In these regions, the surface temperature increase with global warming may lead to dust increase. In some small regional areas only, soil moisture is the dominant factor of the SurDst. The conclusion above applies in April, which is the peak dust season (Fig. 13). Even though some models, such as UKESM1-0-LL, do not show the dominant role of surface air temperature on the SurDst in annual average data, it is more significant in April.

4 Summary and discussion

Using MERRA-2, other reanalysis or observed data, and 9 ESMs from the AerChemMIP of CMIP6, the variations of dust aerosols are explored in this paper. Since 1980, the global mean of MERRA-2 dust concentration at surface significantly increased, which is mainly contributed by the increase of dust outside the core areas of high surface dust concentrations, and surface dust does not show an obvious trend of increase or decrease variations in the core areas. All the 9 ESMs can reasonably reproduce the main characteristics of the spatial distribution of dust aerosol and its seasonal evolutions in the period from 1995 to 2014. Only a few models (such as BCC-ESM1 and GFDL-ESM4) can show a similar dust growth trend of MERRA-2.

Surface wind, air temperature, and soil moisture are important factors for dust variation. Their correlations with dust variation in the period from 1980 to 2020 are analyzed by MERRA-2, ERA-5, GLDAS reanalysis and CRU observation data sets. The relative importance of wind, air temperature, and soil moisture on dust variations are also explored by multiple linear regression. The results are consistent with that using all variables from MERRA-2, and show that:

1. In the dust core areas, surface dust concentration is mainly dominated by the surface wind speed. It is captured by all ESMs.
2. Outside the dust core areas, especially over arid and semiarid regions in middle to high latitudes, surface air temperature warming is the main factor to account for dust increase. As the surface air temperature warming causes the increase in the vertical gradient of temperature, enhances atmospheric instability, and triggers more upward motion to bring more dust. The importance of air temperature impact on dust over those regions is simulated in most ESMs.
3. Only in several regions of small areas in low to middle latitudes, moisture is the primary factor to dominate surface dust, such as in East Asia and South Asia, where are generally high soil moistures. In ESMs, dominated regions of soil moisture impact on surface dust are still distributed in several small regions, but there are large divergences among ESMs.

The influence of surface air temperature on the dust that is suggested in this study, can partially explain their significant positive correlation in the regions outside dust core areas, but further experiments for verification are still needed. In addition, there is still a lack of understanding of the reasons for the changes in some local dust, such as

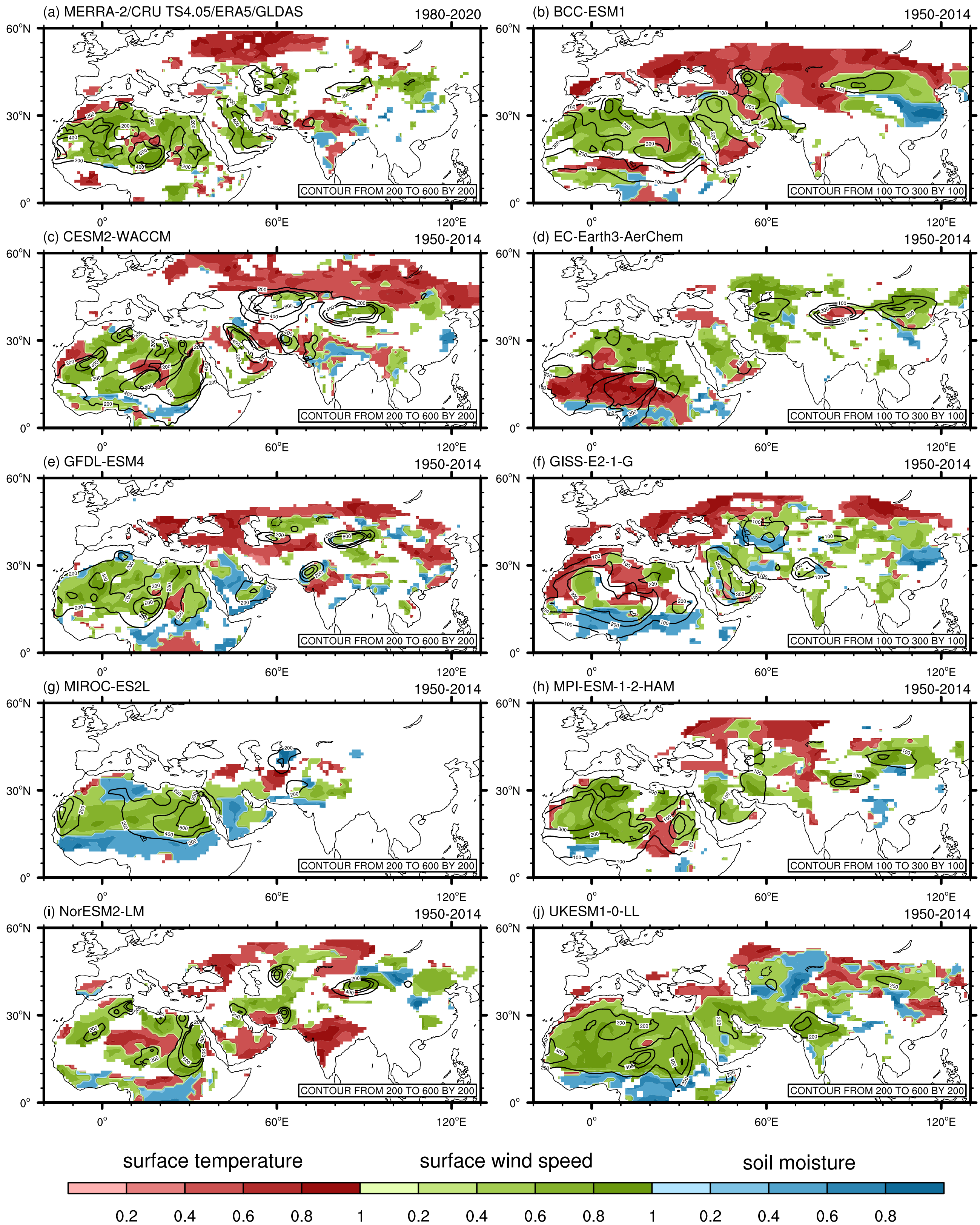

Fig. 13 Same as Fig. 11, but for data in April

the decreasing trend of the SurDst in North and Northeast China. More observation analyses are needed in the future.

Acknowledgements We acknowledge all data developers, their managers and funding agencies for the datasets used in this study, whose work and support are essential to us.

Author contributions All authors contributed to the study conception and design. The main ideas were formulated by TW, YZ, YZ and JZ. The first draft of the manuscript was written by YZ and all authors commented on previous versions of the manuscript. All authors discussed the results and approved the final manuscript.

Funding This work was supported by the National Natural Science Foundation of China (Grant no. 42230608).

Data availability This work uses simulations from 9 ESMs participating in the AerChemMIP of CMIP6 (https://esgf-node.llnl.gov/projects/cmip6/), models information can be found in Table 1. The observation and reanalysis data used in this work are all cited.

Declarations

Conflict of interests The authors have no relevant financial or non-financial interests to disclose.

References

Beaudoing H, Rodell M, NASA/GSFC/HSL (2020), GLDAS Noah Land Surface Model L4 monthly 0.25 × 0.25 degree V2.1, Greenbelt, Maryland, USA, Goddard Earth Sciences Data and Information Services Center (GES DISC). 10.5067/SXAVCZFAQLNO. Accessed 21 Mar 2022

Bauer SE, Tsigaridis K, Faluvegi G, Kelley M, Lo KK, Miller RL, Nazarenko L, Schmidt GA, Wu J (2020) Historical (1850–2014) aerosol evolution and role on climate forcing using the GISS ModelE2.1 contribution to CMIP6. J Adv Model Earth Syst. https://doi.org/10.1029/2019MS001978

Bin Abdulwahed A, Dash J, Roberts G (2019) An evaluation of satellite dust-detection algorithms in the Middle East region. Int J Remote Sens 40:1331–1356. https://doi.org/10.1080/01431161.2018.1524589

Cakmur RV, Miller RL, Perlwitz J, Geogdzhayev IV, Ginoux P, Koch D, Kohfeld KE, Tegen I, Zender CS (2006) Constraining the magnitude of the global dust cycle by minimizing the difference between a model and observations. J Geophys Res 111:D06207. https://doi.org/10.1029/2005JD005791

Chepil WS (1956) Influence of moisture on erodibility of soil by wind. Soil Sci Soc Am J 20:288–292. https://doi.org/10.2136/sssaj1956.03615995002000020033x

Collins WJ, Lamarque J-F, Schulz M, Boucher O, Eyring V, Hegglin MI, Maycock A, Myhre G, Prather M, Shindell D, Smith SJ (2017) AerChemMIP: quantifying the effects of chemistry and aerosols in CMIP6. Geosci Model Dev 10:585–607. https://doi.org/10.5194/gmd-10-585-2017

Danabasoglu G (2019) NCAR CESM2-WACCM model output prepared for CMIP6 CMIP historical. https://doi.org/10.22033/ESGF/CMIP6.10071

Danabasoglu G, Lamarque J-F, Bacmeister J, Bailey DA, DuVivier AK, Edwards J, Emmons LK, Fasullo J, Garcia R, Gettelman A, Hannay C, Holland MM, Large WG, Lauritzen PH, Lawrence DM, Lenaerts JTM, Lindsay K, Lipscomb WH, Mills MJ, Neale R, Oleson KW, Otto-Bliesner B, Phillips AS, Sacks W, Tilmes S, Kampenhout L, Vertenstein M, Bertini A, Dennis J, Deser C, Fischer C, Fox-Kemper B, Kay JE, Kinnison D, Kushner PJ, Larson VE, Long MC, Mickelson S, Moore JK, Nienhouse E, Polvani L, Rasch PJ, Strand WG (2020) The community earth system model version 2 (CESM2). J Adv Model Earth Syst. https://doi.org/10.1029/2019MS001916

Duan H, Hou W, Wu H, Feng T, Yan P (2022) Evolution characteristics of sand-dust weather processes in china during 1961–2020. Front Environ Sci 10:820452. https://doi.org/10.3389/fenvs.2022.820452

Dunne JP, Horowitz LW, Adcroft AJ, Ginoux P, Held IM, John JG, Krasting JP, Malyshev S, Naik V, Paulot F, Shevliakova E, Stock CA, Zadeh N, Balaji V, Blanton C, Dunne KA, Dupuis C, Durachta J, Dussin R, Gauthier PPG, Griffies SM, Guo H, Hallberg RW, Harrison M, He J, Hurlin W, McHugh C, Menzel R, Milly PCD, Nikonov S, Paynter DJ, Ploshay J, Radhakrishnan A, Rand K, Reichl BG, Robinson T, Schwarzkopf DM, Sentman LT, Underwood S, Vahlenkamp H, Winton M, Wittenberg AT, Wyman B, Zeng Y, Zhao M (2020) The GFDL earth system model version 4.1 (GFDL-ESM 4.1): overall coupled model description and simulation characteristics. J Adv Model Earth Syst. https://doi.org/10.1029/2019MS002015

EC-Earth Consortium (EC-Earth) (2020) EC-Earth-Consortium EC-Earth3-AerChem model output prepared for CMIP6 CMIP historical. https://doi.org/10.22033/ESGF/CMIP6.4701

Evans S, Ginoux P, Malyshev S, Shevliakova E (2016) Climate–vegetation interaction and amplification of Australian dust variability. Geophys Res Lett. https://doi.org/10.1002/2016GL071016

Eyring V, Bony S, Meehl GA, Senior CA, Stevens B, Stouffer RJ, Taylor KE (2016) Overview of the Coupled Model Intercomparison Project Phase 6 (CMIP6) experimental design and organization. Geosci Model Dev 9:1937–1958. https://doi.org/10.5194/gmd-9-1937-2016

Filonchyk M (2022) Characteristics of the severe March 2021 Gobi Desert dust storm and its impact on air pollution in China. Chemosphere 287:132219. https://doi.org/10.1016/j.chemosphere.2021.132219

Foltz GR, McPhaden MJ (2008) Trends in Saharan dust and tropical Atlantic climate during 1980–2006. Geophys Res Lett 35:L20706. https://doi.org/10.1029/2008GL035042

Francis D, Nelli N, Fonseca R, Weston M, Flamant C, Cherif C (2022) The dust load and radiative impact associated with the June 2020 historical Saharan dust storm. Atmos Environ 268:118808. https://doi.org/10.1016/j.atmosenv.2021.118808

Fu X, Wang B (2014) Reliability evaluation of soil moisture and land surface temperature simulated by global land data assimilation system (GLDAS) using AMSR-E data. In: Krishnamurti TN, Liu G (eds) Beijing, pp 92650O. https://doi.org/10.1117/12.2074566

Ganor E, Osetinsky I, Stupp A, Alpert P (2010) Increasing trend of African dust, over 49 years, in the eastern Mediterranean. J

Geophys Res 115:D07201. https://doi.org/10.1029/2009JD012500
Gelaro R, McCarty W, Suárez MJ, Todling R, Molod A, Takacs L, Randles CA, Darmenov A, Bosilovich MG, Reichle R, Wargan K, Coy L, Cullather R, Draper C, Akella S, Buchard V, Conaty A, da Silva AM, Gu W, Kim G-K, Koster R, Lucchesi R, Merkova D, Nielsen JE, Partyka G, Pawson S, Putman W, Rienecker M, Schubert SD, Sienkiewicz M, Zhao B (2017) The modern-era retrospective analysis for research and applications, version 2 (MERRA-2). J Clim 30:5419–5454. https://doi.org/10.1175/JCLI-D-16-0758.1
Global Modeling and Assimilation Office (GMAO) (2015) MERRA-2 tavgM_2d_aer_Nx: 2d,Monthly mean, Time-averaged, Single-Level, Assimilation, Aerosol Diagnostics V5.12.4, Greenbelt, MD, USA, Goddard Earth Sciences Data and Information Services Center (GES DISC). 10.5067/FH9A0MLJPC7N. Accessed 20 Jan 2022
Gillette DA, Passi R (1988) Modeling dust emission caused by wind erosion. J Geophys Res 93:14233. https://doi.org/10.1029/JD093iD11p14233
Ginoux P, Chin M, Tegen I, Prospero JM, Holben B, Dubovik O, Lin S-J (2001) Sources and distributions of dust aerosols simulated with the GOCART model. J Geophys Res 106:20255–20273. https://doi.org/10.1029/2000JD000053
Ginoux P, Garbuzov D, Hsu NC (2010) Identification of anthropogenic and natural dust sources using moderate resolution imaging spectroradiometer (MODIS) Deep Blue level 2 data. J Geophys Res 115:D05204. https://doi.org/10.1029/2009JD012398
Ginoux P, Prospero JM, Gill TE, Hsu NC, Zhao M (2012) Global-scale attribution of anthropogenic and natural dust sources and their emission rates based on MODIS Deep Blue aerosol products: anthropogenic and natural dust sources. Rev Geophys. https://doi.org/10.1029/2012RG000388
Goudie AS, Middleton NJ (1992) The changing frequency of dust storms through time. Clim Change 20:197–225. https://doi.org/10.1007/BF00139839
Goudie AS, Middleton NJ (2001) Saharan dust storms: nature and consequences. Earth Sci Rev 56:179–204. https://doi.org/10.1016/S0012-8252(01)00067-8
Grogan DFP, Thorncroft CD (2019) The characteristics of African easterly waves coupled to Saharan mineral dust aerosols. QJR Meteorol Soc 145:1130–1146. https://doi.org/10.1002/qj.3483
Hajima T, Abe M, Arakawa O, Suzuki T, Komuro Y, Ogura T, Ogochi K, Watanabe M, Yamamoto A, Tatebe H, Noguchi MA, Ohgaito R, Ito A, Yamazaki D, Ito A, Takata K, Watanabe S, Kawamiya M, Tachiiri K (2019) MIROC MIROC-ES2L model output prepared for CMIP6 CMIP historical. https://doi.org/10.22033/ESGF/CMIP6.5602
Hajima T, Watanabe M, Yamamoto A, Tatebe H, Noguchi M, Abe M, Ohgaito R, Ito A, Yamazaki D, Okajima H, Ito A, Takata K, Ogochi K, Watanabe S, Kawamiya M (2020) Development of the MIROC-ES2L Earth system model and the evaluation of biogeochemical processes and feedbacks. Geosci Model Dev 13:2197–2244. https://doi.org/10.5194/gmd-13-2197-2020
Hamidi M (2020) The key role of water resources management in the Middle East dust events. CATENA 187:104337. https://doi.org/10.1016/j.catena.2019.104337
Hamidi M, Kavianpour MR, Shao Y (2017) A quantitative evaluation of the 3–8 July 2009 Shamal dust storm. Aeol Res 24:133–143. https://doi.org/10.1016/j.aeolia.2016.12.004
Harris I, Osborn TJ, Jones P, Lister D (2020) Version 4 of the CRU TS monthly high-resolution gridded multivariate climate dataset. Sci Data 7:109. https://doi.org/10.1038/s41597-020-0453-3
Harrison SP, Kohfeld KE, Roelandt C, Claquin T (2001) The role of dust in climate changes today, at the last glacial maximum and in the future. Earth Sci Rev 54:43–80. https://doi.org/10.1016/S0012-8252(01)00041-1
Hersbach H, Bell B, Berrisford P, Biavati G, Horányi A, Muñoz Sabater J, Nicolas J, Peubey C, Radu R, Rozum I, Schepers D, Simmons A, Soci C, Dee D, Thépaut J-N (2019a) ERA5 monthly averaged data on pressure levels from 1979 to present. Copernicus Climate Change Service (C3S) Climate Data Store (CDS). https://doi.org/10.24381/cds.6860a573. Accessed 21 Mar 2022
Hersbach H, Bell B, Berrisford P, Biavati G, Horányi A, Muñoz Sabater J, Nicolas J, Peubey C, Radu R, Rozum I, Schepers D, Simmons A, Soci C, Dee D, Thépaut J-N (2019b) ERA5 monthly averaged data on single levels from 1979 to present. Copernicus Climate Change Service (C3S) Climate Data Store (CDS). https://doi.org/10.24381/cds.f17050d7. Accessed 21 Mar 2022.
Hersbach H, Bell B, Berrisford P, Hirahara S, Horányi A, Muñoz-Sabater J, Nicolas J, Peubey C, Radu R, Schepers D, Simmons A, Soci C, Abdalla S, Abellan X, Balsamo G, Bechtold P, Biavati G, Bidlot J, Bonavita M, Chiara G, Dahlgren P, Dee D, Diamantakis M, Dragani R, Flemming J, Forbes R, Fuentes M, Geer A, Haimberger L, Healy S, Hogan RJ, Hólm E, Janisková M, Keeley S, Laloyaux P, Lopez P, Lupu C, Radnoti G, Rosnay P, Rozum I, Vamborg F, Villaume S, Thépaut J (2020) The ERA5 global reanalysis. QJR Meteorol Soc 146:1999–2049. https://doi.org/10.1002/qj.3803
Hess GD, Spillane KT (1990) Characteristics of dust devils in Australia. J Appl Meteorol 29:498–507. https://doi.org/10.1175/1520-0450(1990)029%3c0498:CODDIA%3e2.0.CO;2
Hess GD, Spillane KT, Lourensz RS (1988) Atmospheric vortices in shallow convection. J Appl Meteorol 27:305–317. https://doi.org/10.1175/1520-0450(1988)027%3c0305:AVISC%3e2.0.CO;2
Horowitz LW, Naik V, Paulot F, Ginoux PA, Dunne JP, Mao J, Schnell J, Chen X, He J, John JG, Lin M, Lin P, Malyshev S, Paynter D, Shevliakova E, Zhao M (2020) The GFDL global Atmospheric Chemistry-Climate Model AM4.1: model description and simulation characteristics. J Adv Model Earth Syst. https://doi.org/10.1029/2019MS002032
Indoitu R, Orlovsky L, Orlovsky N (2012) Dust storms in Central Asia: spatial and temporal variations. J Arid Environ 85:62–70. https://doi.org/10.1016/j.jaridenv.2012.03.018
IPCC (2022) Climate Change 2022: Mitigation of Climate Change. Contribution of Working Group III to the Sixth Assessment Report of the Intergovernmental Panel on Climate Change. In: Shukla PR, Skea J, Slade R, Al Khourdajie A, van Diemen R, McCollum D, Pathak M, Some S, Vyas P, Fradera R, Belkacemi M, Hasija A, Lisboa G, Luz S, Malley J (eds) Cambridge University Press, Cambridge. https://doi.org/10.1017/9781009157926
Jiang Y, Han S, Shi C, Gao T, Zhen H, Liu X (2021) Evaluation of HRCLDAS and ERA5 datasets for near-surface wind over Hainan Island and South China Sea. Atmosphere 12:766. https://doi.org/10.3390/atmos12060766
Karim R, Tan G, Ayugi B, Babaousmail H, Liu F (2020) Evaluation of historical CMIP6 model simulations of seasonal mean temperature over Pakistan during 1970–2014. Atmosphere 11:1005. https://doi.org/10.3390/atmos11091005
Kędzior M, Zawadzki J (2016) Comparative study of soil moisture estimations from SMOS satellite mission, GLDAS database, and cosmic-ray neutrons measurements at COSMOS station in Eastern Poland. Geoderma 283:21–31. https://doi.org/10.1016/j.geoderma.2016.07.023
Kelley M, Schmidt GA, Nazarenko LS, Bauer SE, Ruedy R, Russell GL, Ackerman AS, Aleinov I, Bauer M, Bleck R, Canuto V, Cesana G, Cheng Y, Clune TL, Cook BI, Cruz CA, Del Genio AD, Elsaesser GS, Faluvegi G, Kiang NY, Kim D, Lacis AA, Leboissetier A, LeGrande AN, Lo KK, Marshall J, Matthews EE, McDermid S, Mezuman K, Miller RL, Murray LT, Oinas V, Orbe C, García-Pando CP, Perlwitz JP, Puma MJ, Rind D, Romanou

A, Shindell DT, Sun S, Tausnev N, Tsigaridis K, Tselioudis G, Weng E, Wu J, Yao M (2020) GISS-E2.1: configurations and climatology. J Adv Model Earth Syst. https://doi.org/10.1029/2019MS002025

Kirkevåg A, Grini A, Olivié D, Seland Ø, Alterskjær K, Hummel M, Karset IHH, Lewinschal A, Liu X, Makkonen R, Bethke I, Griesfeller J, Schulz M, Iversen T (2018) A production-tagged aerosol module for Earth system models, OsloAero5.3—extensions and updates for CAM5.3-Oslo. Geosci Model Dev 11:3945–3982. https://doi.org/10.5194/gmd-11-3945-2018

Krasnov H, Katra I, Friger M (2016) Increase in dust storm related PM10 concentrations: a time series analysis of 2001–2015. Environ Pollut 213:36–42. https://doi.org/10.1016/j.envpol.2015.10.021

Krasting JP, John JG, Blanton C, McHugh C, Nikonov S, Radhakrishnan A, Rand K, Zadeh NT, Balaji V, Durachta J, Dupuis C, Menzel R, Robinson T, Underwood S, Vahlenkamp H, Dunne KA, Gauthier PP, Ginoux P, Griffies SM, Hallberg R, Harrison M, Hurlin W, Malyshev S, Naik V, Paulot F, Paynter DJ, Ploshay J, Reichl BG, Schwarzkopf DM, Seman CJ, Silvers L, Wyman B, Zeng Y, Adcroft A, Dunne JP, Dussin R, Guo H, He J, Held IM, Horowitz LW, Lin P, Milly PCD, Shevliakova E, Stock C, Winton M, Wittenberg AT, Xie Y, Zhao M (2018) NOAA-GFDL GFDL-ESM4 model output prepared for CMIP6 CMIP historical. https://doi.org/10.22033/ESGF/CMIP6.8597

Ledari DG, Hamidi M, Shao Y (2022) Numerical simulation of the 18 February 2017 frontal dust storm over southwest of Iran using WRF-Chem, satellite imagery, and PM10 concentrations. J Arid Environ 196:104637. https://doi.org/10.1016/j.jaridenv.2021.104637

Liu X, Ma P-L, Wang H, Tilmes S, Singh B, Easter RC, Ghan SJ, Rasch PJ (2016) Description and evaluation of a new four-mode version of the Modal Aerosol Module (MAM4) within version 5.3 of the Community Atmosphere Model. Geosci Model Dev 9:505–522. https://doi.org/10.5194/gmd-9-505-2016

MalAmiri N, Rashki A, Hosseinzadeh SR, Kaskaoutis DG (2022) Mineralogical, geochemical, and textural characteristics of soil and airborne samples during dust storms in Khuzestan, southwest Iran. Chemosphere 286:131879. https://doi.org/10.1016/j.chemosphere.2021.131879

Marticorena B, Bergametti G (1995) Modeling the atmospheric dust cycle: 1. Design of a soil-derived dust emission scheme. J Geophys Res 100:16415. https://doi.org/10.1029/95JD00690

Mbourou GN, Bertrand JJ, Nicholson SE (1997) The diurnal and seasonal cycles of wind-borne dust over Africa North of the Equator. J Appl Meteorol 36:868–882. https://doi.org/10.1175/1520-0450(1997)036%3c0868:TDASCO%3e2.0.CO;2

McKenna-Neuman C, Nickling WG (1989) A theoretical and wind tunnel investigation of the effect of capillary water on the entrainment of sediment by wind. Can J Soil Sci 69:79–96. https://doi.org/10.4141/cjss89-008

Middleton NJ (1985) Effect of drought on dust production in the Sahel. Nature 316:431–434. https://doi.org/10.1038/316431a0

Middleton NJ, Goudie AS (2001) Saharan dust: sources and trajectories. Trans Inst Br Geogr 26:165–181. https://doi.org/10.1111/1475-5661.00013

Middleton N, Kang U (2017) Sand and dust storms: impact mitigation. Sustainability 9:1053. https://doi.org/10.3390/su9061053

Miller RL, Cakmur RV, Perlwitz J, Geogdzhayev IV, Ginoux P, Koch D, Kohfeld KE, Prigent C, Ruedy R, Schmidt GA, Tegen I (2006) Mineral dust aerosols in the NASA Goddard Institute for Space Sciences ModelE atmospheric general circulation model. J Geophys Res 111:D06208. https://doi.org/10.1029/2005JD005796

Mirzabaev A, Wu J, Evans J, García-Oliva F, Hussein IAG, Iqbal MH, Kimutai J, Knowles T, Meza F, Nedjraoui D, Tena F, Türkeş M, Vázquez RJ, Weltz M (2019) Desertification. In: Shukla PR, Skea J, Calvo Buendia E, Masson-Delmotte V, Pörtner H-O, Roberts DC, Zhai P, Slade R, Connors S, van Diemen R, Ferrat M, Haughey E, Luz S, Neogi S, Pathak M, Petzold J, Portugal Pereira J, Vyas P, Huntley E, Kissick K, Belkacemi M, Malley J (eds) Climate Change and Land: an IPCC special report on climate change, desertification, land degradation, sustainable land management, food security, and greenhouse gas fluxes in terrestrial ecosystems (**In press**)

Mukkavilli SK, Prasad AA, Taylor RA, Huang J, Mitchell RM, Troccoli A, Kay MJ (2019) Assessment of atmospheric aerosols from two reanalysis products over Australia. Atmos Res 215:149–164. https://doi.org/10.1016/j.atmosres.2018.08.026

Mulcahy JP, Johnson C, Jones CG, Povey AC, Scott CE, Sellar A, Turnock ST, Woodhouse MT, Abraham NL, Andrews MB, Bellouin N, Browse J, Carslaw KS, Dalvi M, Folberth GA, Glover M, Grosvenor DP, Hardacre C, Hill R, Johnson B, Jones A, Kipling Z, Mann G, Mollard J, O'Connor FM, Palmiéri J, Reddington C, Rumbold ST, Richardson M, Schutgens NAJ, Stier P, Stringer M, Tang Y, Walton J, Woodward S, Yool A (2020) Description and evaluation of aerosol in UKESM1 and HadGEM3-GC3.1 CMIP6 historical simulations. Geosci Model Dev 13:6383–6423. https://doi.org/10.5194/gmd-13-6383-2020

Munson SM, Belnap J, Okin GS (2011) Responses of wind erosion to climate-induced vegetation changes on the Colorado Plateau. Proc Natl Acad Sci USA 108:3854–3859. https://doi.org/10.1073/pnas.1014947108

NASA Goddard Institute for Space Studies (NASA/GISS) (2018) NASA-GISS GISS-E2.1G model output prepared for CMIP6 CMIP historical. https://doi.org/10.22033/ESGF/CMIP6.7127

Neubauer D, Ferrachat S, Siegenthaler-Le Drian C, Stoll J, Folini DS, Tegen I, Wieners K-H, Mauritsen T, Stemmler I, Barthel S, Bey I, Daskalakis N, Heinold B, Kokkola H, Partridge D, Rast S, Schmidt H, Schutgens N, Stanelle T, Stier P, Watson-Parris D, Lohmann U (2019) HAMMOZ-Consortium MPI-ESM1.2-HAM model output prepared for CMIP6 CMIP historical. https://doi.org/10.22033/ESGF/CMIP6.5016

Notaro M, Yu Y, Kalashnikova OV (2015) Regime shift in Arabian dust activity, triggered by persistent Fertile Crescent drought. J Geophys Res Atmos. https://doi.org/10.1002/2015JD023855

Prospero JM, Ginoux P, Torres O, Nicholson SE, Gill TE (2002) Environmental characterization of global sources of atmospheric soil dust identified with the nimbus 7 total ozone mapping spectrometer (toms) absorbing aerosol product: global sources of atmospheric soil dust. Rev Geophys 40:2-1–2-31. https://doi.org/10.1029/2000RG000095

Prospero JM, Barkley AE, Gaston CJ, Gatineau A, Campos y Sansano A, Panechou K (2020) Characterizing and quantifying African dust transport and deposition to South America: implications for the phosphorus budget in the Amazon Basin. Glob Biogeochem Cycles. https://doi.org/10.1029/2020GB006536

Qin W, Liu Y, Wang L, Lin A, Xia X, Che H, Bilal M, Zhang M (2018) Characteristic and driving factors of aerosol optical depth over Mainland China during 1980–2017. Remote Sens 10:1064. https://doi.org/10.3390/rs10071064

Rami A, Hamidi M, Neya BN (2022) Atmospheric analysis of dust storms in Sistan region. J Atmos Solar Terr Phys 227:105800. https://doi.org/10.1016/j.jastp.2021.105800

Randles CA, da Silva AM, Buchard V, Colarco PR, Darmenov A, Govindaraju R, Smirnov A, Holben B, Ferrare R, Hair J, Shinozuka Y, Flynn CJ (2017) The MERRA-2 aerosol reanalysis, 1980 onward. Part I: system description and data assimilation evaluation. J Clim 30:6823–6850. https://doi.org/10.1175/JCLI-D-16-0609.1

Rienecker MM, Suarez MJ, Gelaro R, Todling R, Bacmeister J, Liu E, Bosilovich MG, Schubert SD, Takacs L, Kim G-K, Bloom S, Chen J, Collins D, Conaty A, da Silva A, Gu W, Joiner J, Koster

RD, Lucchesi R, Molod A, Owens T, Pawson S, Pegion P, Redder CR, Reichle R, Robertson FR, Ruddick AG, Sienkiewicz M, Woollen J (2011) MERRA: NASA's modern-era retrospective analysis for research and applications. J Clim 24:3624–3648. https://doi.org/10.1175/JCLI-D-11-00015.1

Rodell M, Houser PR, Jambor U, Gottschalck J, Mitchell K, Meng C-J, Arsenault K, Cosgrove B, Radakovich J, Bosilovich M, Entin JK, Walker JP, Lohmann D, Toll D (2004) The Global land data assimilation system. Bull Am Meteorol Soc 85:381–394. https://doi.org/10.1175/BAMS-85-3-381

Roshan DR, Koc M, Isaifan R, Shahid MZ, Fountoukis C (2019) Aerosol optical thickness over large urban environments of the Arabian Peninsula—speciation, variability, and distributions. Atmosphere 10:228. https://doi.org/10.3390/atmos10050228

Schepanski K, Tegen I, Macke A (2012) Comparison of satellite based observations of Saharan dust source areas. Remote Sens Environ 123:90–97. https://doi.org/10.1016/j.rse.2012.03.019

Seland Ø, Bentsen M, Olivié D, Toniazzo T, Gjermundsen A, Graff LS, Debernard JB, Gupta AK, He Y-C, Kirkevåg A, Schwinger J, Tjiputra J, Aas KS, Bethke I, Fan Y, Griesfeller J, Grini A, Guo C, Ilicak M, Karset IHH, Landgren O, Liakka J, Moseid KO, Nummelin A, Spensberger C, Tang H, Zhang Z, Heinze C, Iversen T, Schulz M (2020) Overview of the Norwegian Earth System Model (NorESM2) and key climate response of CMIP6 DECK, historical, and scenario simulations. Geosci Model Dev 13:6165–6200. https://doi.org/10.5194/gmd-13-6165-2020

Seland Ø, Bentsen M, Olivè DJL, Toniazzo T, Gjermundsen A, Graff LS, Debernard JB, Gupta AK, He Y, Kirkevåg A, Schwinger J, Tjiputra J, Aas KS, Bethke I, Fan Y, Griesfeller J, Grini A, Guo C, Ilicak M, Karset I, Landgren OA, Liakka J, Moseid KO, Nummelin A, Spensberger C, Tang H, Zhang Z, Heinze C, Iversen T, Schulz M (2019) NCC NorESM2-LM model output prepared for CMIP6 CMIP historical. https://doi.org/10.22033/ESGF/CMIP6.8036

Sellar AA, Jones CG, Mulcahy JP, Tang Y, Yool A, Wiltshire A, O'Connor FM, Stringer M, Hill R, Palmieri J, Woodward S, Mora L, Kuhlbrodt T, Rumbold ST, Kelley DI, Ellis R, Johnson CE, Walton J, Abraham NL, Andrews MB, Andrews T, Archibald AT, Berthou S, Burke E, Blockley E, Carslaw K, Dalvi M, Edwards J, Folberth GA, Gedney N, Griffiths PT, Harper AB, Hendry MA, Hewitt AJ, Johnson B, Jones A, Jones CD, Keeble J, Liddicoat S, Morgenstern O, Parker RJ, Predoi V, Robertson E, Siahaan A, Smith RS, Swaminathan R, Woodhouse MT, Zeng G, Zerroukat M (2019) UKESM1: description and evaluation of the U.K. earth system model. J Adv Model Earth Syst 11:4513–4558. https://doi.org/10.1029/2019MS001739

Shao Y, Klose M, Wyrwoll K-H (2013) Recent global dust trend and connections to climate forcing: GLOBAL DUST TREND. J Geophys Res Atmos 118:11107–11118. https://doi.org/10.1002/jgrd.50836

Shi L, Zhang J, Yao F, Zhang D, Guo H (2021) Drivers to dust emissions over dust belt from 1980 to 2018 and their variation in two global warming phases. Sci Total Environ 767:144860. https://doi.org/10.1016/j.scitotenv.2020.144860

Sissakian VK, Al-Ansari N, Knutsson S (2013) Sand and dust storm events in Iraq. NS 05:1084–1094. https://doi.org/10.4236/ns.2013.510133

Song H, Zhang K, Piao S, Wan S (2016) Spatial and temporal variations of spring dust emissions in northern China over the last 30 years. Atmos Environ 126:117–127. https://doi.org/10.1016/j.atmosenv.2015.11.052

Takemura T (2005) Simulation of climate response to aerosol direct and indirect effects with aerosol transport-radiation model. J Geophys Res 110:D02202. https://doi.org/10.1029/2004JD005029

Takemura T, Okamoto H, Maruyama Y, Numaguti A, Higurashi A, Nakajima T (2000) Global three-dimensional simulation of aerosol optical thickness distribution of various origins. J Geophys Res 105:17853–17873. https://doi.org/10.1029/2000JD900265

Takemura T, Egashira M, Matsuzawa K, Ichijo H, O'ishi R, Abe-Ouchi A (2009) A simulation of the global distribution and radiative forcing of soil dust aerosols at the Last Glacial Maximum. Atmos Chem Phys 9:3061–3073. https://doi.org/10.5194/acp-9-3061-2009

Tang Y, Rumbold S, Ellis R, Kelley D, Mulcahy J, Sellar A, Walton J, Jones C (2019) MOHC UKESM1.0-LL model output prepared for CMIP6 CMIP historical. https://doi.org/10.22033/ESGF/CMIP6.6113

Tegen I, Harrison SP, Kohfeld K, Prentice IC, Coe M, Heimann M (2002) Impact of vegetation and preferential source areas on global dust aerosol: results from a model study: GLOBAL DUST AEROSOL MODEL. J Geophys Res. https://doi.org/10.1029/2001JD000963

Tegen I, Neubauer D, Ferrachat S, Siegenthaler-Le Drian C, Bey I, Schutgens N, Stier P, Watson-Parris D, Stanelle T, Schmidt H, Rast S, Kokkola H, Schultz M, Schroeder S, Daskalakis N, Barthel S, Heinold B, Lohmann U (2019) The global aerosol–climate model ECHAM6.3–HAM2.3—part 1: aerosol evaluation. Geosci Model Dev 12:1643–1677. https://doi.org/10.5194/gmd-12-1643-2019

Tsunematsu N, Kuze H, Sato T, Hayasaki M, Cui F, Kondoh A (2011) Potential impact of spatial patterns of future atmospheric warming on Asian dust emission. Atmos Environ 45:6682–6695. https://doi.org/10.1016/j.atmosenv.2011.08.048

Ukhov A, Mostamandi S, da Silva A, Flemming J, Alshehri Y, Shevchenko I, Stenchikov G (2020) Assessment of natural and anthropogenic aerosol air pollution in the Middle East using MERRA-2, CAMS data assimilation products, and high-resolution WRF-Chem model simulations. Atmos Chem Phys 20:9281–9310. https://doi.org/10.5194/acp-20-9281-2020

University of East Anglia Climatic Research Unit, Harris IC, Jones PD, Osborn T (2021) CRU TS4.05: Climatic Research Unit (CRU) Time-Series (TS) version 4.05 of high-resolution gridded data of month-by-month variation in climate (Jan. 1901–Dec. 2020). NERC EDS Centre for Environmental Data Analysis. https://catalogue.ceda.ac.uk/uuid/c26a65020a5e4b80b20018f148556681. Accessed 19 Mar 2022

van Noije TPC, Le Sager P, Segers AJ, van Velthoven PFJ, Krol MC, Hazeleger W, Williams AG, Chambers SD (2014) Simulation of tropospheric chemistry and aerosols with the climate model EC-Earth. Geosci Model Dev 7:2435–2475. https://doi.org/10.5194/gmd-7-2435-2014

van Noije T, Bergman T, Le Sager P, O'Donnell D, Makkonen R, Gonçalves-Ageitos M, Döscher R, Fladrich U, von Hardenberg J, Keskinen J-P, Korhonen H, Laakso A, Myriokefalitakis S, Ollinaho P, Pérez García-Pando C, Reerink T, Schrödner R, Wyser K, Yang S (2021) EC-Earth3-AerChem: a global climate model with interactive aerosols and atmospheric chemistry participating in CMIP6. Geosci Model Dev 14:5637–5668. https://doi.org/10.5194/gmd-14-5637-2021

Veselovskii I, Goloub P, Podvin T, Tanre D, da Silva A, Colarco P, Castellanos P, Korenskiy M, Hu Q, Whiteman DN, Pérez-Ramírez D, Augustin P, Fourmentin M, Kolgotin A (2018) Characterization of smoke and dust episode over West Africa: comparison of MERRA-2 modeling with multiwavelength Mie-Raman lidar observations. Atmos Meas Tech 11:949–969. https://doi.org/10.5194/amt-11-949-2018

Wang F, Yang T, Wang Z, Cao J, Liu B, Liu J, Chen S, Liu S, Jia B (2021) A Comparison of the different stages of dust events over Beijing in March 2021: the effects of the vertical structure on near-surface particle concentration. Remote Sens 13:3580. https://doi.org/10.3390/rs13183580

Woodward S (2001) Modeling the atmospheric life cycle and radiative impact of mineral dust in the Hadley Centre climate model. J Geophys Res 106:18155–18166. https://doi.org/10.1029/2000JD900795

Wu T, Zhang F, Zhang J, Jie W, Zhang Y, Wu F, Li L, Yan J, Liu X, Lu X, Tan H, Zhang L, Wang J, Hu A (2020a) Beijing Climate Center Earth System Model version 1 (BCC-ESM1): model description and evaluation of aerosol simulations. Geosci Model Dev 13:977–1005. https://doi.org/10.5194/gmd-13-977-2020

Wu X, Li X, Li J, Wang M, Ji M, Cao Y, Hu J, Zhang P (2020b) Eolian dust activity during the last ~850 years on the southeastern margin of the arid Central Asia. Palaeogeogr Palaeoclimatol Palaeoecol 560:110022. https://doi.org/10.1016/j.palaeo.2020.110022

Xu Y, Zhao P, Si D, Cao L, Wu X, Zhao Y, Liu N (2020) Development and preliminary application of a gridded surface air temperature homogenized dataset for China. Theor Appl Climatol 139:505–516. https://doi.org/10.1007/s00704-019-02972-z

Yao W, Che H, Gui K, Wang Y, Zhang X (2020) Can MERRA-2 reanalysis data reproduce the three-dimensional evolution characteristics of a typical dust process in East Asia? A case study of the dust event in May 2017. Remote Sens 12:902. https://doi.org/10.3390/rs12060902

Yao W, Gui K, Wang Y, Che H, Zhang X (2021) Identifying the dominant local factors of 2000–2019 changes in dust loading over East Asia. Sci Total Environ 777:146064. https://doi.org/10.1016/j.scitotenv.2021.146064

Yousefi R, Wang F, Ge Q, Shaheen A (2020) Long-term aerosol optical depth trend over Iran and identification of dominant aerosol types. Sci Total Environ 722:137906. https://doi.org/10.1016/j.scitotenv.2020.137906

Zender CS (2003) Mineral dust entrainment and deposition (DEAD) model: description and 1990s dust climatology. J Geophys Res 108:4416. https://doi.org/10.1029/2002JD002775

Zhang XY, Gong SL, Zhao TL, Arimoto R, Wang YQ, Zhou ZJ (2003) Sources of Asian dust and role of climate change versus desertification in Asian dust emission: ASIAN DUST SOURCES. Geophys Res Lett. https://doi.org/10.1029/2003GL018206

Zhang J, Wu T, Shi X, Zhang F, Li J, Chu M, Liu Q, Yan J, Ma Q, Wei M (2018) BCC BCC-ESM1 model output prepared for CMIP6 CMIP historical. https://doi.org/10.22033/ESGF/CMIP6.2949

Zhao A, Ryder CL, Wilcox LJ (2022) How well do the CMIP6 models simulate dust aerosols? Atmos Chem Phys 22:2095–2119. https://doi.org/10.5194/acp-22-2095-2022

Zhu C, Wang B, Qian W (2008) Why do dust storms decrease in northern China concurrently with the recent global warming? Geophys Res Lett 35:L18702. https://doi.org/10.1029/2008GL034886

Zhu J, Xie A, Qin X, Wang Y, Xu B, Wang Y (2021) An assessment of ERA5 reanalysis for Antarctic near-surface air temperature. Atmosphere 12:217. https://doi.org/10.3390/atmos12020217

Zong Q, Mao R, Gong D-Y, Wu C, Pu B, Feng X, Sun Y (2021) Changes in dust activity in spring over East Asia under a global warming scenario. Asia Pac J Atmos Sci 57:839–850. https://doi.org/10.1007/s13143-021-00224-7